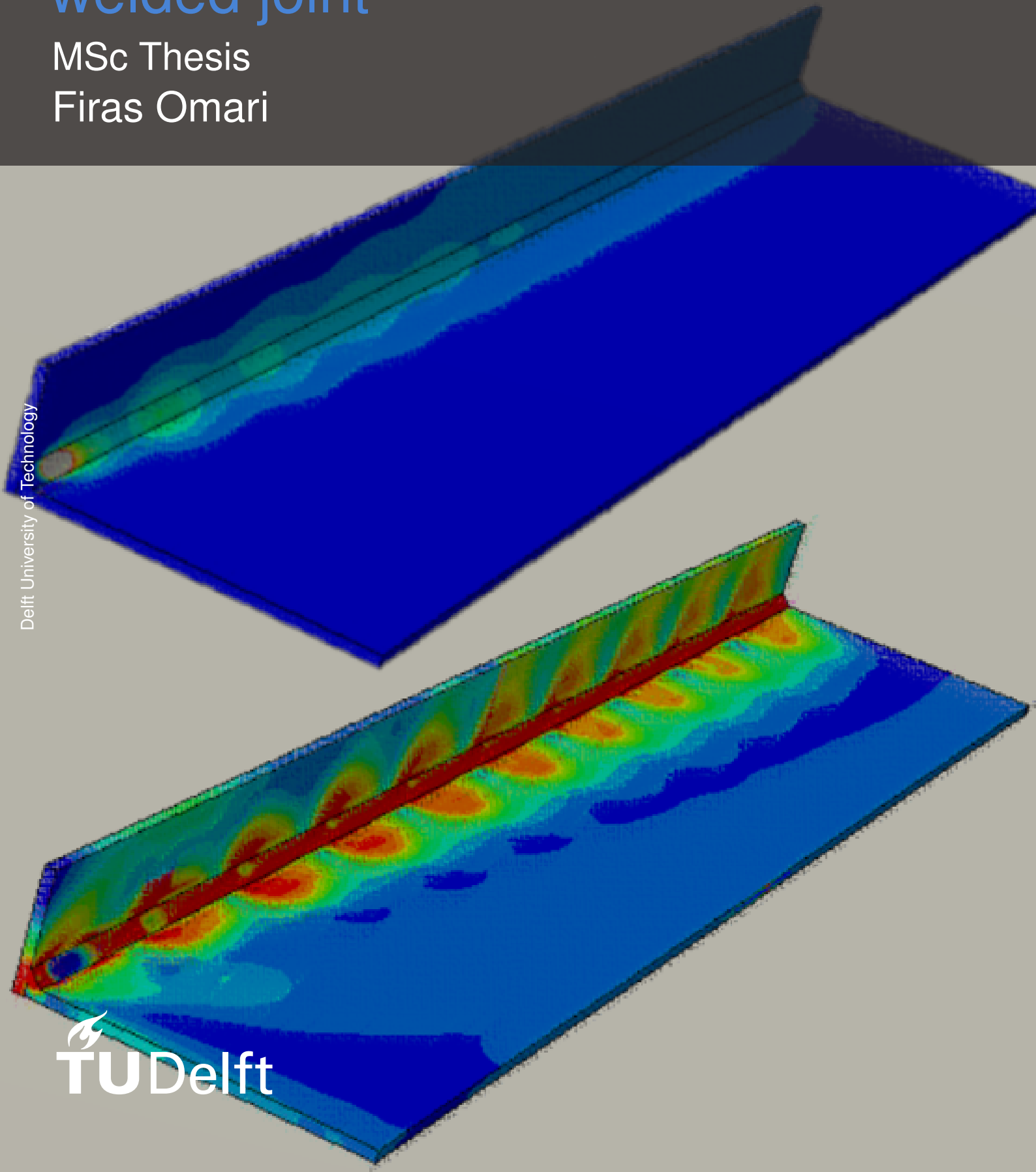


Evolution of the welding residual stresses after cutting of a cruciform welded joint

MSc Thesis
Firas Omari

Delft University of Technology



Evolution of the welding residual stresses after cutting of a cruciform welded joint

by

Firas Omari

Student Name	Student Number
Firas Omari	5149290

Thesis submitted to Delft University of Technology for the degree of
Master of Science
in Civil Engineering
to be publicly defended on 14/12/2022 at 12:30 pm.

Instructor:	Prof.dr. Milan Veljkovic	TU Delft, Chair
	Prof.dr.ir Johan Maljaars	TNO
	Dr.Ing. H.M. Slot	TNO, Daily supervisor
	Dr.Ir. A. Mohabeddine	TU Delft, Daily supervisor
Institution:	Delft University of Technology	
Place:	Faculty of Civil Engineering, Delft	
Project Duration:	February, 2022 - December, 2022	

An electronic version of this thesis is available at <http://repository.tudelft.nl>.

Preface

This project is the last chapter of my student life at the faculty of Civil Engineering at Delft University of Technology. I have been a student non-stop my whole life and this thesis has been the most challenging yet the most beneficial project I have ever worked on.

I am very proud of what I have achieved and managed to learn the past couple of months. These kind of projects are not done to just learn about a certain engineering topic and master it, it is way beyond that; it's a process where you learn to believe in yourself. It's a process that gives you a spark that makes you believe that you can solve any problem you can face. I have grown professionally as well as personally, and a big part of that goes to my graduation committee from TU Delft and TNO. I am very thankful for having to collaborate with them as they have shared so many beneficial experiences and knowledge with me. I admire their work and their passion to always aim for the best results.

As much as I am thankful for the constant support of my friends throughout the hard times, it would have been more efficient without them in terms of time and money.. but as I was stuck with them in the faculty, I have enjoyed every single moment with them and it would have been impossible to get the motivation to keep up the good work. To my beloved country, Palestine. I hope all the youth build themselves incredibly, so we can rebuild the damage and raise our voice to the world. An educated generation is the one to bridge the gaps and help in the cause. Last but not least, to my sisters, Haya and Reem, and my parents, Wisam and Abdul Naser. There are no words that can comprehend how lucky I am to have you by my side in everything that I face. You have been patient although I made you broke, you have been supportive, loving and fun. Thanks for believing in me.

TU Delft is an unforgettable experience, but I'm looking forward for the next one!

Firas Omari
Delft, December 2022

Summary

The use of welding is widely adopted to assemble structural components in the construction industry for many years. To ensure safety of these welded components, many fatigue tests have been conducted on many different shapes and configurations of welded connections to precisely assess the fatigue life. However, testing real-size structures and specimens is very limited due to its high cost and in-applicability. Thus, these full scale specimens are cut down into small scale specimens to allow applicability for testing. Different characteristics are exhibited between the full and the small scale specimens, as there are major difference in residual stresses induced by welding and cutting, which may give non conservative predictions for fatigue life.

In this thesis, the objective is to forecast the evolution of the residual stress field originated by welding of a full scale and small scale specimens of a cruciform joint at the weld toe after breaking it down into smaller specimens using a cutting process by performing a numerical analysis using Abaqus finite element analysis software.

To achieve this goal, first, a thermo-mechanical welding simulation was performed to obtain a welding residual stress field on a 910 mm long cruciform joint, which is done in two main parts, starting with the thermal model in which a temperature field is analysed. The temperature field from the thermal model is used as an input for the mechanical model in which the residual stress field is produced due to the temperature change and restriction of movement of material due to the shrinkage and expansion.

Secondly, the 910 mm long full-scale cruciform joint was cut into five shorter specimens of 500, 210, 120, 75, and 20 mm. The welding residual stress (WRS) levels at the weld toe for each specimen was recorded and showed large stress losses and relaxations as the specimen gets shorter in length. a major longitudinal stress loss of 97% and 77% loss of maximum principle stresses when cutting down the 910 to a 20 mm long specimen, making it almost free of WRS, but only a 5-6% loss of longitudinal and Max. principal stresses when going from 910 to 500 mm.

Thirdly, after generating multiple welded specimens with different lengths, a tension load of 186.2 is set in the x-direction of the attachment plate of the cruciform joint, and the stress level at the weld toe was analysed due to the applied load and the WRS. A 40% increase of the stress occur due to the applied load, but a very slight decrease in longitudinal stresses for the 910, 500 and 210 mm due to depicting a plate-like behaviour in contraction due to poisson's effect.

Finally, the same specimens were analysed under the 186.2 MPa load but without including the WRS. Different shapes of stress distributions were found, and differences in stresses when comparing the models with and without WRS in the models. The difference in longitudinal z-direction reached up to 282 MPa, while only 77 MPa in the transverse direction. The maximum principle stresses insured the importance of including WRS when performing fatigue assessment as it showed the fatigue failure to occur in the weld root with a crack to happen at the middle part. The specimens that exclude WRS would start cracking at the edges of the weld root, but in the central part of the weld seam when including WRS. The model that included WRS showed similar fracture location at the weld root as the fractured specimen performed in tests at TNO's laboratories.

The next steps in this research is the modification of a modelling methods. The results can be improved and smoothed by modelling using the effective notch method were a radius is introduced at the weld toe and the root to eliminate the stress singularities. The welding simulation can be improved to get better results by modelling the full cruciform joint without symmetry conditions, and include a weld order for all four welds with proper cooling time in between each weld.

Contents

Preface	i
Summary	ii
List of Figures	v
List of Tables	viii
1 Introduction	1
1.1 Background and Problem definition	1
1.2 Research Objective.	3
1.3 Research Question and Sub-Questions.	3
1.4 Methodology	4
1.5 Research Structure.	5
2 Literature review	6
2.1 Fatigue physics	6
2.2 Size effect.	7
2.2.1 Specimen size effect on fatigue	8
2.2.2 Welded cruciform joint specimens	8
2.3 Welding Residual Stresses.	9
2.3.1 Formation of residual stresses.	9
2.3.2 Effect on fatigue resistance	10
2.3.3 Relaxation due to cutting and machining	11
2.3.4 Relaxation due to loading	12
3 Welding simulation analysis	13
3.1 Welding Simulation.	13
3.1.1 Thermal model	14
3.1.2 Mechanical model	20
4 Cutting of the full scale specimen	25
4.1 FE model for the cutting process	25
4.1.1 Cutting Process Boundary conditions	26
4.2 Welding residual stress evolution	27
4.2.1 Longitudinal WRS evolution	27
4.2.2 Transverse WRS evolution	30
4.2.3 Max Principle stress evolution	32
4.3 Loading of welded specimens	34
4.3.1 Longitudinal Stress	34
4.3.2 Transverse Stress	38
4.3.3 2D plane stress validation	41
4.3.4 Maximum Principle Stress	43
4.3.5 Fractured surface after fatigue testing	45
5 Conclusions and recommendations	48
5.1 Possible improvements	48
5.2 Conclusions.	49
5.3 Recommendations	50

- References** **52**
- A Appendix A: DFLUX code** **53**
- B Appendix B: Python Code for Element Sets** **55**
 - B.1 Thermal Model 55
 - B.2 Mechanical model 56

List of Figures

1.1	Varying stress distributions of machined cruciform joints along the weld seam of different specimen sizes after machining.	1
1.2	Flowchart to answer the main question	4
2.1	Fatigue life stages [1]	6
2.2	Fatigue strength at 2 million cycles as a function of weld seam length [12]	7
2.3	load path in a load-carrying (right) vs. non-load-carrying cruciform joints (left)	9
2.4	Local plastic deformations in the weld [1]	9
2.5	Formation of residual stresses in butt weld	10
2.6	residual and applied stress range on the effective stress range [20]	11
2.7	Cutting width effects on residual stress distributions at the WT: (a) LWRS; (b) TWRS [11]	11
3.1	1/4 cruciform joint model - simplification	14
3.2	Cruciform joint cross section	14
3.3	Material Properties	15
3.4	Stress-strain per temperature	16
3.5	10 element sets along the length of the weld	16
3.6	Heat source model [26]	17
3.7	Weld dimensions	17
3.8	Heat model weld	18
3.9	Heat affected zone	18
3.10	Mechanical Boundary Conditions	20
3.11	Mesh	21
3.12	Temperature between weld increments	21
3.13	LWRS Stress discontinuities	22
3.14	TWRS Stress discontinuities	22
3.15	23
3.16	Longitudinal stress relaxation after BC removal	23
3.17	Longitudinal σ_z welding residual stress along weld toe	23
3.18	Transverse σ_x welding residual stress along weld toe	24
3.19	Maximum Principle welding residual stress along weld toe	24
4.1	Chapter 4 flowchart	25
4.2	Abaqus restart analysis	26
4.3	Schematic of the 910 mm long specimen step-by-step cutting process	26
4.4	Boundary conditions representation for the cutting process	27
4.5	Full scale 910 mm	27
4.6	Small scale 500 mm	27
4.7	Small scale 210 mm	28
4.8	Small scale 120 mm	28
4.9	Small scale 75 mm	28
4.10	Small scale 20 mm	28
4.11	Evolution of LWRS due to cutting	28
4.12	Decreasing trend of LWRS	29
4.13	Full scale 910 mm	30
4.14	Small scale 500 mm	30
4.15	Small scale 210 mm	30
4.16	Small scale 120 mm	30
4.17	Small scale 75 mm	30

4.18 Small scale 20 mm	30
4.19 Evolution of TWRS due to cutting	31
4.20 Trend of TWRS	31
4.21 Full scale 910 mm	32
4.22 Small scale 500 mm	32
4.23 Small scale 210 mm	32
4.24 Small scale 120 mm	32
4.25 Small scale 75 mm	32
4.26 Small scale 20 mm	32
4.27 Evolution of Max. Principle stress due to cutting	33
4.28 Decreasing trend of Max principle WRS	33
4.29 Tension loading	34
4.30 Full scale 910 mm	34
4.31 Small scale 500 mm	34
4.32 Small scale 210 mm	35
4.33 Small scale 120 mm	35
4.34 Small scale 75 mm	35
4.35 Small scale 20 mm	35
4.36 WRS vs. WRS and Loading for 910, 500 and 210 mm	35
4.37 WRS vs. WRS and Loading for 120, 75 and 20 mm	35
4.38 Longitudinal stress due to load only	36
4.39 Deformation in z-direction for 20 mm specimen	36
4.40 Deformation in z-direction for 910 mm specimen	36
4.41 WRS & Load vs. Load only for (910, 500 and 210mm)	37
4.42 WRS & Load vs. Load only for (120, 75 and 20 mm)	37
4.43 Full scale 910 mm	38
4.44 Small scale 500 mm	38
4.45 Small scale 210 mm	38
4.46 Small scale 120 mm	38
4.47 Small scale 75 mm	38
4.48 Small scale 20 mm	38
4.49 WRS vs. WRS and Loading for 910, 500 and 210 mm	39
4.50 WRS vs. WRS and Loading for 120, 75 and 20 mm	39
4.51 Transverse stress due to load only	40
4.52 Deformation in x-direction for 20 mm specimen	40
4.53 WRS & Load vs. Load only for (910, 500 and 210mm)	40
4.54 WRS & Load vs. Load only for (120, 75 and 20 mm)	40
4.55 2D plane stress & plane strain in a 3D	41
4.56 2D Plane stress model	42
4.57 3D model	42
4.58 Full scale 910 mm	43
4.59 Small scale 500 mm	43
4.60 Small scale 210 mm	43
4.61 Small scale 120 mm	43
4.62 Small scale 75 mm	43
4.63 Small scale 20 mm	43
4.64 Max. Principle stress flow at the weld root	44
4.65 Mesh refinement	44
4.66 Effective notch method at root	44
4.67 Max. Principle stress flow for the 20 mm	45
4.68 Dimensions of the 120 mm long cruciform joint specimen	46
4.69 Fatigue testing at TNO laboratories	46
4.70 Detected crack initiation with simple photography test by TNO [12]	46
4.71 Max. Principle stress flow due to Load only for the 120 mm	47
4.72 Max. Principle stress flow due to load and WRS for the 120 mm	47

5.1 Improved mechanical boundary conditions compared to figure 3.10 48

List of Tables

3.1	Unit heat input model	15
3.2	Welding properties for the cruciform joint	17
3.3	Maximum compressive stress comparison between weld ends	24
4.1	Maximum longitudinal tensile and compressive stresses along weld toe	29
4.2	Longitudinal stress loss from full scale to small scale specimen comparison	29
4.3	Maximum Transverse tensile and compressive stresses along weld toe	31
4.4	Transverse stress loss from full scale to small scale specimen comparison	31
4.5	Maximum Principle tensile and compressive stresses along weld toe	33
4.6	Maximum Principle stress loss from full scale to small scale specimen comparison	33
4.7	Difference in peak stress when including and excluding LWRS in FEA	37
4.8	Longitudinal vs. Transverse stress due to load and welding	39
4.9	Difference in peak stress when including and excluding TWRS in FEA	40
4.10	3D vs 2D plane stress	41

1

Introduction

1.1. Background and Problem definition

Welding of metals is widely used in construction as there is a wide use of welded components that are applied mainly in steel bridges, marine structures, pipelines, ships and many others. In the late 1930s, before the use of welding, connections in these structures were riveted. There are several reasons why welded structures are superior to riveted ones, including greater strength, weight reduction, simplicity of design, and quick fabrication. However, despite its convenience, welded components exhibit a complex behaviour and are prone to distortions and fatigue damage when subjected under fluctuating loads. Thus, they require a deep understanding. [1]

Tensile residual stresses are significant features of fatigue damage in welded components [2]. Any free-standing body must maintain stress equilibrium, which calls for a compressive stress elsewhere in the body to counteract the presence of a tensile residual stress in the component. Tensile residual stresses are undesirable stresses formed during the welding when manufacturing components, with values that can reach yield stress which can cause the initial fatigue cracks to remain open, which also accelerates the rate of crack propagation [3].

Fatigue is often a major problem limiting the load-carrying capacity and residual life of steel welded structures. Avoiding such a problem can be done by planned inspection routines, successful strengthening techniques and identifying correct fatigue-prone details, which can guarantee an adequate performance of structures during their service life. Knowledge about the fatigue performance of specific structural details is of a great importance for engineers and designers, as it can help in giving a better estimation of maintenance time and cost [4].

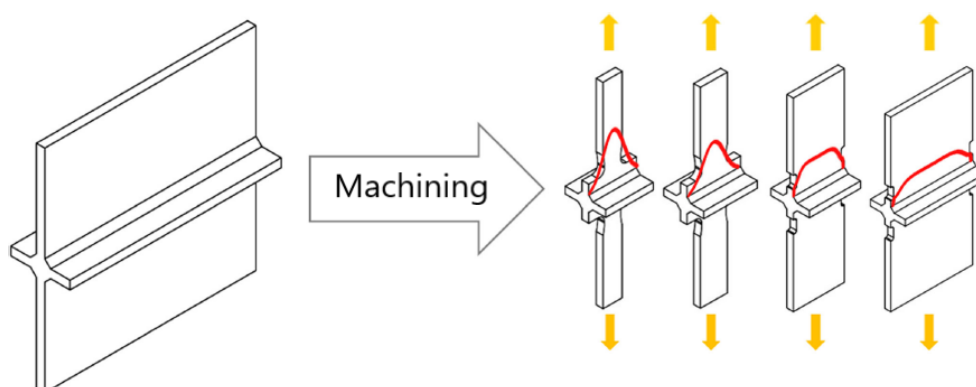


Figure 1.1: Varying stress distributions of machined cruciform joints along the weld seam of different specimen sizes after machining.

Fatigue failure mostly appear in welded connections rather than in the base material. Thus, fatigue tests and analysis on welded connections needs to be carried out. Many welded connections have

a complex and very large configurations under complex variable loading, which limits the scope for performing fatigue tests on full scale welded structures under real loading conditions. Fatigue tests for lifetime estimation of full-scale structures can be extremely expensive and generally not applicable. Hence, it is sufficient to breakdown the full-scale into small-scale specimens to make it applicable for testing as shown in figure 1.1.

Gathering knowledge in terms of data scatter and fatigue strength on full-scale using small-scale specimens is ambiguous, as they exhibit different characteristics when it comes to fatigue strength. The difference in fatigue strength is in part attributed in residual stress originated from manufacturing process of welding and cutting [5]. The standards of fatigue design [6, 7, 8, 9, 10] build S-N curves for fatigue life assessment based on tests of small scale specimens, and those specimens are subjected to stress relief in relevant directions can lead to an underestimation of the effective stress ranges experienced by the full-scale structures. Thus unsafe estimations of fatigue lives may be obtained from small-scale specimens.

The mechanical cutting procedure is typically employed to remove the welded joint specimens for the laboratory from the welded structure. Therefore, a thorough analysis of the welding residual stress distributions using mechanical cutting can help with precise fatigue testing in the laboratory and further enhance the security of welded parts [11].

1.2. Research Objective

Following the above investigation, aiding the engineers and designers to have a better knowledge on the performance of welded connections and understanding of the stress state distributions for different specimen sizes is a triumph. To do this, it is necessary to address the issue of the paucity of the study on the subject of welding residual stress redistribution when cutting full-scale specimens of welded connections into small-scale specimens, which would provide a platform to help understand the effect of the distribution of the welding residual stress on the fatigue performance

As the manufacturing process creates residual stresses in the joints due to welding and cutting, The goal of this study is forecasting the evolution of the residual stress field originated by welding of full and small scale specimens of a load-carrying cruciform joint specimen at the weld toe after cutting into smaller specimens by performing numerical analysis using ABAQUS FEA.

1.3. Research Question and Sub-Questions

The main research question is formulated to tackle the research objective and problem statement. It is expressed as followed:

How does the distribution of the welding residual stresses at the weld toe for welded joints change when cutting full-scale to small-scale specimens?

The main question can be broken down into sub-questions:

1. What is the residual stress field distribution for a 910 mm long full-scale cruciform joint specimen?
2. How is the welding residual stress at the weld toe changed when cutting a full-scale cruciform joint into smaller specimen?
3. What is the contribution of the welding residual stress levels when assessing fatigue?

1.4. Methodology

A literature review was performed to gather the necessary background information on the topic. Alongside the literature review, The FEA software Abaqus was studied and presented densely in this thesis. Reports from TNO experiments [12] were provided to compare numerical and experimental results in terms of fracture location. The main question and sub-questions were answered by following the steps shown in figure 1.2

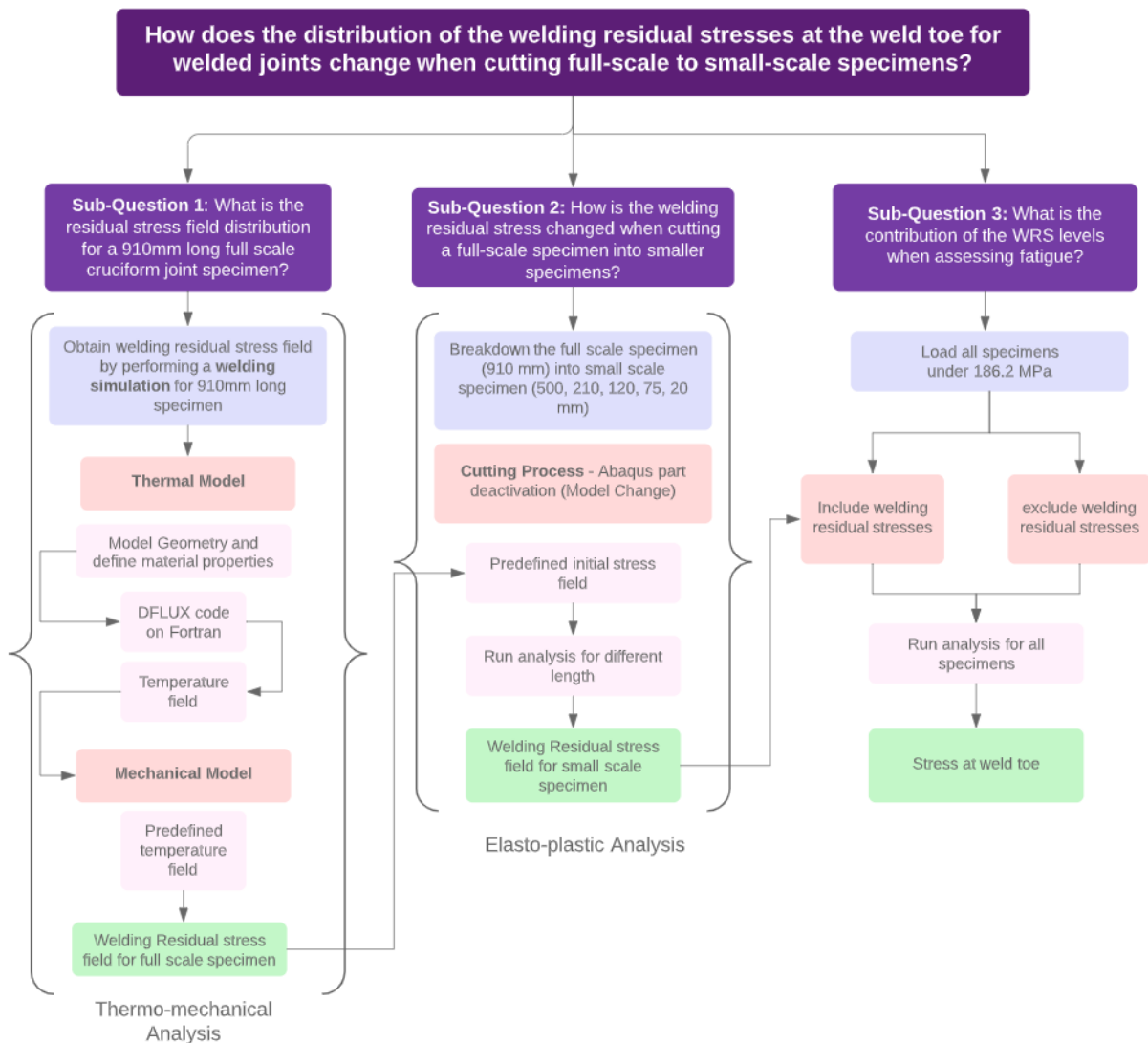


Figure 1.2: Flowchart to answer the main question

Sub-question 1 is answered by performing a welding simulation that consists of a thermal model which produces a temperature field to be used as an input for the mechanical model to generate a welding residual stress for a 910 mm full scale cruciform joint specimen with specified mechanical boundary conditions that is over restricted in some parts.

Sub-question 2 is answered by cutting the 910 mm long full scale specimen after welding into small scale specimens of 500, 210, 120, 75, and 20mm using part deactivation feature in Abaqus FEA. The stress level difference at the weld toe is analysed.

Sub-question 3 is answered by loading all the specimens with a load of 186.2 MPa. To be able to assess the welding residual stress contribution on the different specimens when loaded for fatigue tests, a numerical analysis on the specimens including and excluding welding residual stresses is performed. The stress distributions and a comparison of the crack site initiation between TNO's experimental results

with the numerical results for the 120 mm specimen.

1.5. Research Structure

In order to keep the thesis well organised, it is divided into five main chapters. The structure is described below.

- **Chapter 1**, Presents the Introduction, research objective, research questions and the used methodology.
- **Chapter 2**, A literature review is presented. It presents the main information about fatigue of welded connections and precisely the crack initiation in welds due to applied cyclic loading. An important section in this chapter is the effect cutting of welded joints into different lengths on the redistribution of stresses. The main information about welding residual stresses and finally, the main principles of plane stress and plane strain and how they vary along lengths and thicknesses.
- **Chapter 3**, A thermo-mechanical welding simulation for a full scale 910 mm long cruciform specimen is presented. A welding induced residual stress field is generated throughout the whole specimen by initially obtaining a temperature field using for a thermal model. The results of the temperature field is then used as an input for the mechanical model to generate residual stresses caused by the temperature change and the restriction of movement of material due to shrinkage and expansion in the elements.
- **Chapter 4**, The cutting process of the full scale 910 mm long specimen to multiple small scale specimens is presented. An elasto-plastic analysis is performed by using a compatible model and mesh orientations as from the welding simulation to generate 5 small scale specimens. The welding residual stress field at the weld toe is analysed and discussed. The effect of the WRS on the fatigue performance is then analysed by loading all the specimens with models that include and exclude WRS.
- **Chapter 5** presents the main conclusions and recommendations of the total work.

2

Literature review

This chapter gathers the most relevant information for this research. Firstly, the most general information regarding fatigue physics that discusses the crack initiation and propagation phases in the fatigue life. The effect of the length of the weld seam and a comparison of full and small scale specimens is presented. The welding residual stresses regarding its formation process, its effect on fatigue and the relaxation due to cutting and loading is presented.

2.1. Fatigue physics

Fatigue is the degradation mechanism in a material when a cyclic loading is applied and becomes visible in the form of cracks. The start of the micro-cracks will grow bigger to eventually lead to a complete failure of the structures at the end of the fatigue life called fracture [13]. Thus, the calculated life of fatigue of a structure is measured in terms of number of cycles that it can withstand.

The fatigue life consists of two different stages, the crack initiation and crack propagation stage. The occurrence of the crack is at the stage of the crack initiation, which has a slow pace of crack growth and the crack at this starts by a cyclic slip mechanism. When the crack continuous growing into the material, the cyclic slip is restrained by the surrounding material. The crack propagation or crack growth starts as the growth mechanism changes, and the growth rate increases until it reaches the fracture toughness where the brittle failure due to fracture occurs.

These two different stages must be looked at separately since there are many different dependencies and properties for each stage. The crack initiation depends is related to the stress concentration factor K_t , the crack propagation is related to the stress intensity factor K , and the final fracture is related to the fracture toughness K_{Ic} . The fatigue life stages can be seen in figure 2.1.

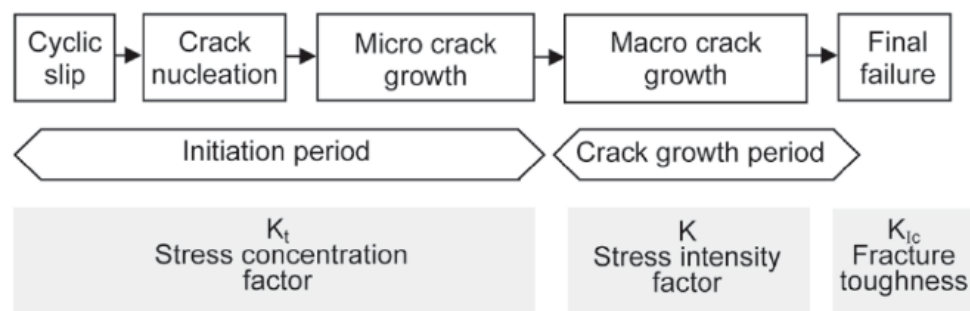


Figure 2.1: Fatigue life stages [1]

The crack initiation stage is a consequence of a cyclic slip, which implies a plastic deformation, or in other words dislocation activities. This phenomenon occurs when the cyclic shear stress amplitudes are lower than the yield stress of the material. The crack initiation can start due to many reasons such as surface roughness, damage and treatment, environmental effects, etc. Any flaw on the surface of

the material can be a reason to start a crack, thus the surface condition is usually the cause for crack initiation [13].

Stress concentration factors has to be taken into consideration in this stage, as high levels of stress occurs at the geometrical discontinuities at the surface. So the maximum stress value at the discontinuity is found by multiplying the stress concentration factor K_t with the nominal stress σ_{nom} .

$$\sigma_{max} = K_t \sigma_{nom} \quad (2.1)$$

Such geometrical discontinuities can occur in different forms, especially when it comes to welded connections, which is the focus of this thesis; the welding process creates residual stresses and exhibits a variety of imperfections at and around the weld region, more details are presented in section 2.3.

2.2. Size effect

The size effect in the fatigue behaviour of structural components, by which fatigue strength decreases as the size of the component increases, is relevant. This can be seen in statistical studies that the number and severity of defects tend to be higher with increase of size, and also in terms of the effect of related dimensions on any geometric stress concentration present.

For members loaded in bending, the fatigue strength increases with increasing stress gradient, so for a high stress gradient in a thin plate gives a higher fatigue strength compared to a thick plate with the same stress gradient. [2] This is the same for welded joints, but the difference is that the focus here is in the welded joints dimensions on stress concentrations [2]. As explained by [14], a longer weld length gives a larger probability of a less good local geometry and a larger possible defect that reduces the fatigue capacity.

A large data base was collected by [12] from different sources, shows different weld lengths for different welded geometries such as butt welds, tube flange and cruciform specimens against the fatigue strength at 2 million cycles. Figure 2.2 shows the decrease of fatigue strength as a function of weld seam length.

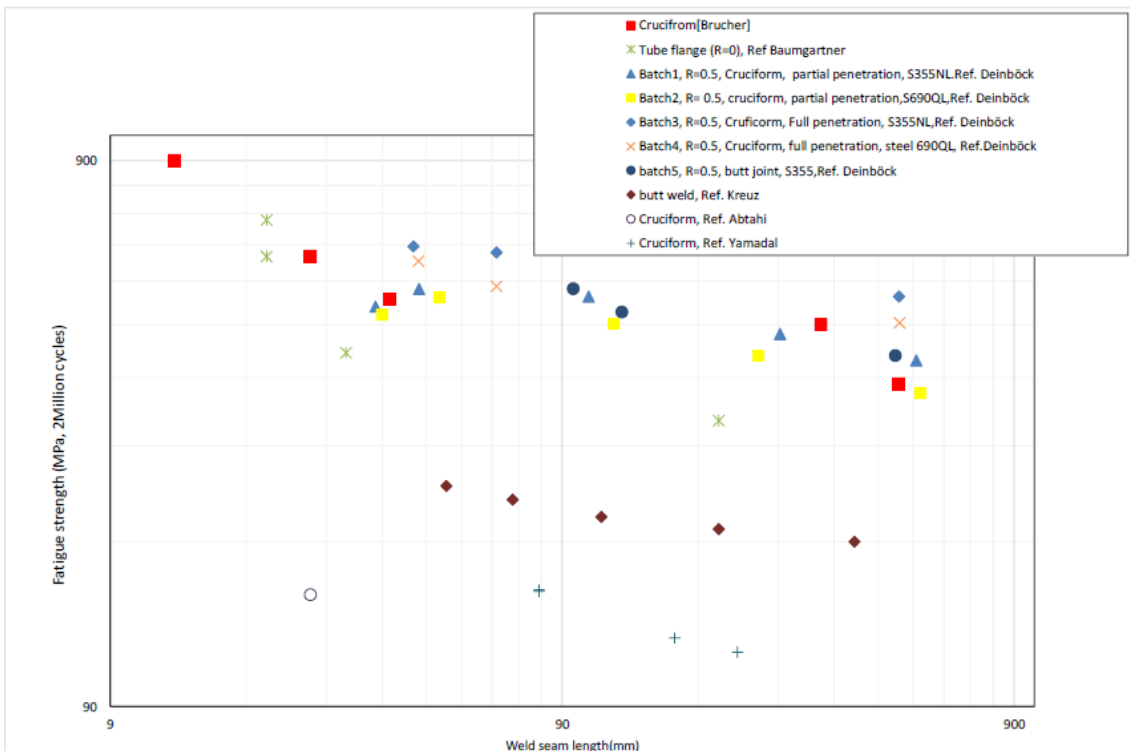


Figure 2.2: Fatigue strength at 2 million cycles as a function of weld seam length [12]

A dominant factor effecting the fatigue performance of a welded joint with different specimen lengths is the residual stresses around and at the weld region. The research of [11] focuses on evaluating

the fatigue performance for a cruciform welded joint that is cut into shorter sections by quantifying the residual stress contribution as a fracture driving force to determine the stress intensity factor K , which is used to estimate the number of cycles for each specimen length using the Paris law. The longitudinal and transverse welding residual stresses gradually decreased with the reduction of welded joint length. The peak value of the tensile residual stresses decreased by 18% as the length was cut from 160 mm to 120 mm. The fatigue life is higher for the 120 mm long specimen as the stress intensity factor (K) decreased from 1.44 to 1.20, thus higher number of cycles.

2.2.1. Specimen size effect on fatigue

The test results of mainly small-scale specimens of structural details are utilized to create the S-N curves in the design standards [6, 7, 8, 9, 10] that are used to perform fatigue life assessments of full scale steel ship, offshore and infrastructures. The behaviour between full-scale structures and small-scale specimens is completely different as they exhibit incompatible characteristics when it comes to fatigue performance. However, S-N curves are often built using small scale data for pragmatic purposes.

Full scale specimens are local structural components within full scale structures. Due to the high cost and limited use of full-scale specimen testing, these full-scale specimens are broken down into smaller specimens. However, given the differences in characteristics between the full and the small-scale specimens, it is uncertain whether small-scale specimens can accurately predict the fatigue lifetime of large-scale structures without taking major conservatism into account. A major part when inspecting the fatigue properties between the full and the small-scale specimens is the difference of residual stresses, which is a big factor when considering the characteristics of fatigue [15]. When constructing the S-N curves and establishing the relevant knowledge on fatigue from laboratory testing, a pertinent information is gathered from small-scale specimen, which have been relieved from internal stresses can result in underestimating of the effective stress levels that the full-scale structure must endure [15].

Ohta and Maeda [15] stated that the testing with an applied stress ratio of $R = 0$ is typically used to determine the fatigue strength of welded joints. Real welded structures do, however, usually have large tensile residual stresses. It follows that the fatigue strength of large-scale welded parts does not change as a result of the stress ratio. High tensile residual stress causes this insensitivity to stress ratio to exist. The impact of a tensile residual stress is to raise the effective mean stress. In welded parts, shakedown happens readily because the combined tensile residual stress and applied stress are greater than the material's yield strength. As a result, regardless of stress ratio, the actual maximum stress in a large-scale welded member equals the yield strength.

Small-scale specimens have lower residual stress levels than full-scale structures, which results in a longer fatigue life in the results of small-scale fatigue tests, which is implicitly assumed by fatigue design guidelines. This would indicate that the fatigue lifespan of the full-scale structures that are developed in accordance with the standards based on the findings of these small-scale tests were estimated improperly. To reduce this un-conservatism, fatigue design guidelines recommend testing new small-scale specimens at a higher load ratio.

2.2.2. Welded cruciform joint specimens

In cruciform welded joints, it is crucial to initially distinguish between a load-carrying and non-load-carrying types. A cruciform joint that is not designed to transmit loads to the main members is said to be non-load-carrying. A load-carrying cruciform joint, on the other hand, transfers load from one member to the other. Figure 2.3 shows the load path of both, and in most cases the fatigue cracks in the non-load-carrying joints are initiated from the weld toes, but in load-carrying joints, fatigue cracks can be initiated from the weld roots as well as the weld toes.

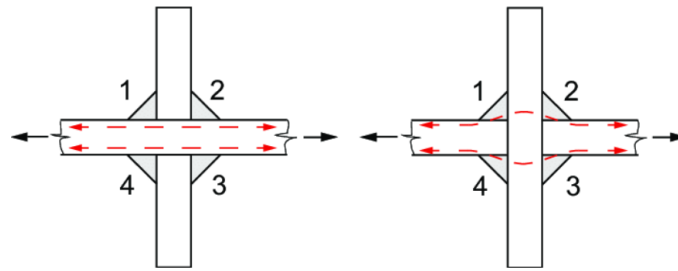


Figure 2.3: load path in a load-carrying (right) vs. non-load-carrying cruciform joints (left)

As mentioned, the fatigue design standards assume that the small scale specimen have lower welding residual stresses than the full-scale ones, which gives different fatigue life estimation results. However, contradictory findings of residual stress differences have been found by in-situ strain gauge measurements on small-scale fillet welded cruciform specimens (cut from a larger plate). These measurements showed that the residual stresses at the weld toe perpendicular to the weld (transverse welding stresses) are higher in the small size specimens for fillet welded cruciform joints. This goes against the fatigue guidelines implicit presumption that residual stress will be relieved in relation to the hot spot [5].

2.3. Welding Residual Stresses

Residual stresses are stresses that appear and remain in an object even in the absence of external loading or thermal gradients [16]. During the manufacturing of steel elements, residual stresses are generally introduced into the materials. The welding process of steel elements also creates high residual stresses that occur within the specimen by initially heating it by a weld arc. The filler material that is used to connect the steel plates together acts almost like a liquid as the stiffness of the material is very low at these high temperatures. Once the filler material and the material surrounding the weld cools down, the material shrinks and stiffens and the movement is not anymore free. These restrained shrinkage causes tensile residual stress in the weld region.

2.3.1. Formation of residual stresses

High local temperatures are caused by the moving heat source during the welding process. The material expands as a result of the high temperature. Compressive stresses and plastic deformations emerge as a result of the surrounding, cooler material's restriction on expansion. Figure 2.4 shows the local plastic deformations around the heat source. Compressive plastic deformations are developed at the front part of the heat source, and tensile plastic deformations develop behind the heat source due to the restricted shrinkage during cooling. The tensile residual stress is caused by the plastic shrinkage that stays inside the weld/

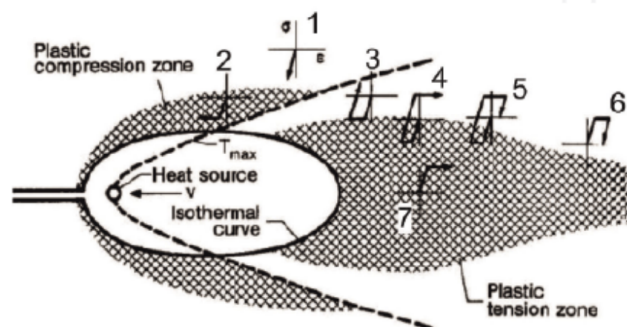


Figure 2.4: Local plastic deformations in the weld [1]

The process of welding creates high residual stresses around the weld region, but there can be different reasons for the occurrence of residual stresses. According to [17] there are three major reasons

for the development of residual stresses during manufacturing:

1. Plastic deformation
2. Phase transformation
3. Thermal gradient

It is a natural condition that these residual stresses are balanced within a body of a material; by way of explanation, there is an equilibrium between tensile and compressive stresses as shown in figure 2.5 (b). The formation process of the residual stresses is presented in figure 2.5 (a) in which it is inhibited due to the restraining effect of the adjacent material at lower temperature. The longitudinal shrinkage is resisted during cooling, as illustrated in (b), and the weld may adjust its "unnatural" length through plastic strain [18].

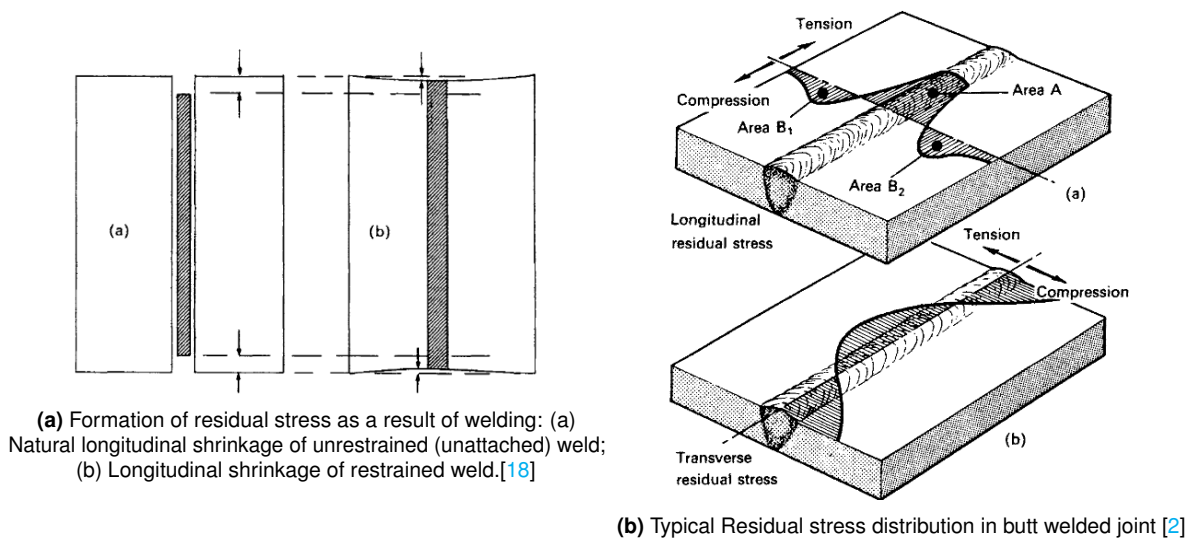


Figure 2.5: Formation of residual stresses in butt weld

2.3.2. Effect on fatigue resistance

The tensile residual stress reduces the fatigue life by speeding up the crack formation process during the initiation and the propagation stages. The remaining compressive stresses are favorable for fatigue life as they increase both fatigue strength and resistance to stress-corrosion cracking [11, 1, 19].

The mean of the effective stress range applied is highly influenced by the tensile residual stress, as it increases it. the tensile stress in the effective stress range is contributor of the fatigue damage . It is defined as the sum of the applied stress range and the residual stress as shown in equation 2.2.

$$\sigma_{mean} = \sigma_{applied} + \sigma_{residual} \quad (2.2)$$

If the welded specimen is applied under fully compressive loading, the fatigue damage would still occur because of the high tensile residual stresses induced by the welding process. For multiple internal stress circumstances along with a tension-only fatigue loading, the effective stress range is shown in figure 2.6. The degree of residual stress close to the yield stress is taken into account in design standards like Eurocode 3 part 1-9, but not the actual stress or the impact of the mean stress. The Eurocode fatigue life calculation is conservative when the mean load is compressive.

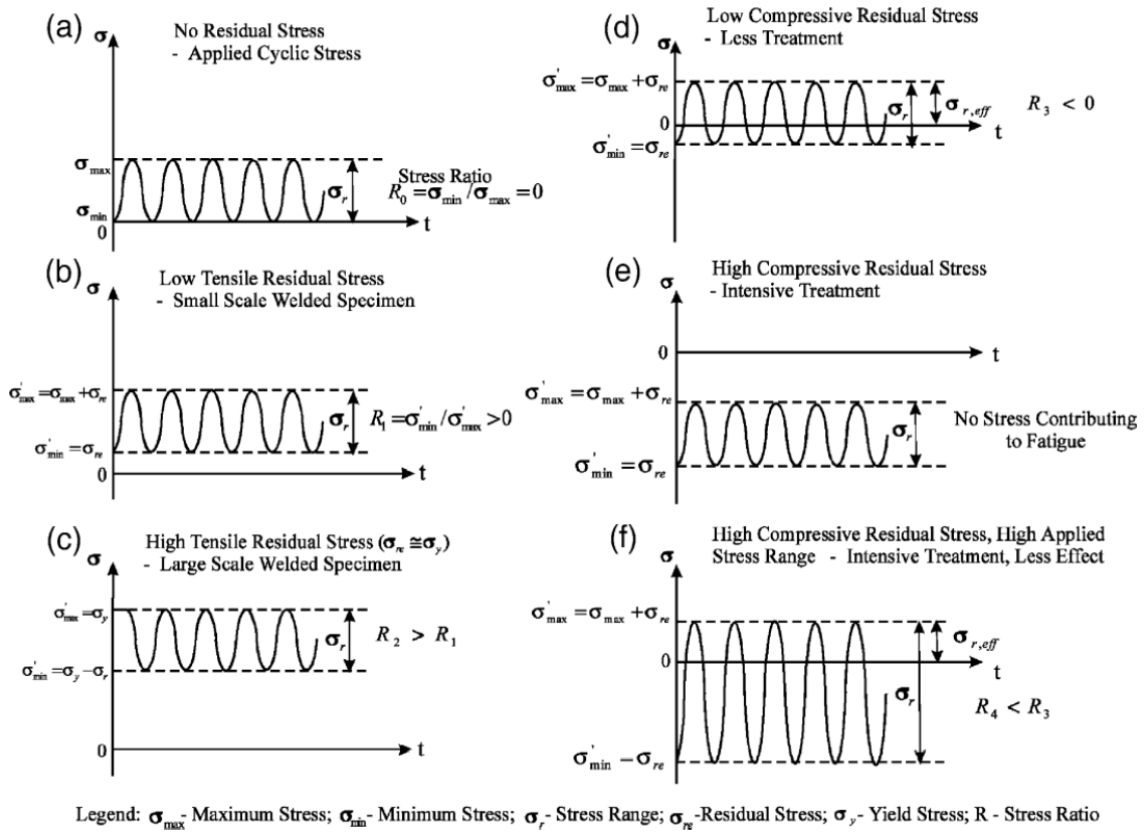


Figure 2.6: residual and applied stress range on the effective stress range [20]

2.3.3. Relaxation due to cutting and machining

According to [11], for a non-load-carrying cruciform joint with steel plates of S355 J2, The longitudinal welding residual stresses(LWRS) and transverse welding residual stresses (TWRS) measured at the weld toe relax after the cutting process. A 160 mm specimen was welded and cut down into sections of different widths, were the peak value of the tensile residual stress and the high value tensile residual stress range decreased with each width. The distribution of the LWRS when cutting the 160 mm specimen to 120 mm, a decrease of 18% occur when going from a peak stress of 511 to 418 MPa. while the TWRS decrease from 271 MPa to 221 MPa, which is a decrease of 18.4%. When the joint is further cut into 80 mm and then to 24mm, the stress decrease by 44% and 81.8% respectively; the compressive stress also goes with the same trend as the tensile stresses.

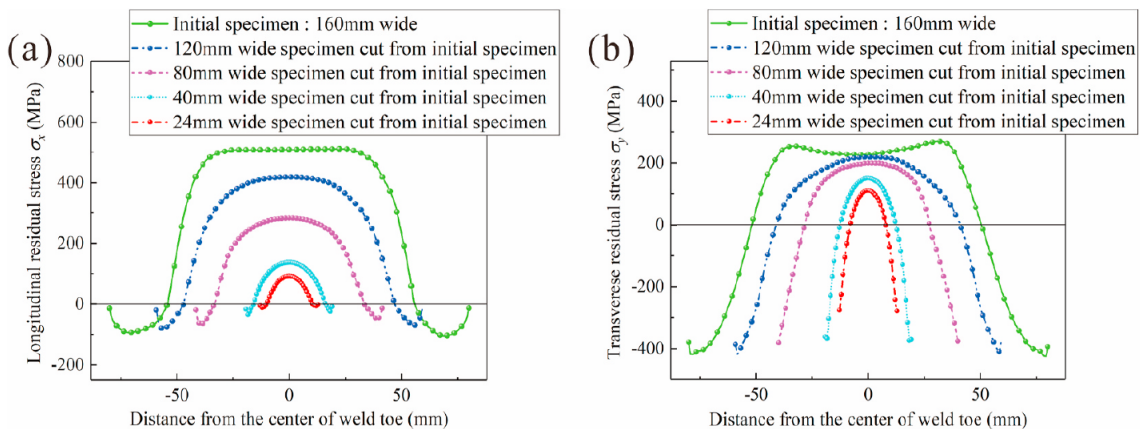


Figure 2.7: Cutting width effects on residual stress distributions at the WT: (a) LWRS; (b) TWRS [11]

2.3.4. Relaxation due to loading

In different locations along the weld seam, there are varying tensile and compressive stresses that are in equilibrium. The residual stress distribution has a great impact on the fatigue resistance and should be considered in the fatigue assessment. As the fatigue loading is applied, there are re-distributions and relaxation in the residual stresses [21]. A relaxation of stress can reach up to 45-60% of the maximum residual stress during the first cycle under fatigue loading because of the plastic deformation caused by the superposition between the as-weld residual stress and the applied load, and the greater the stress amplitude and cyclic number, the more residual stresses are released, but can be limited [22]. The relaxation phenomenon due to the applied load is complex and depend on various factors including the loading type and scenario, number of cycles and material properties.

3

Welding simulation analysis

This chapter presents a welding simulation for a 910 mm long cruciform joint specimen to generate a welding residual stress field using a Finite Element Analysis software, ABAQUS 2021 [23]. The welding simulation process is done using a thermo-mechanical analysis, thus divided into two main phases, starting with the thermal model analysis that is performed in which the heat transfer of the welding arc to the specimen is found, and ending with a mechanical model which uses the output of the thermal model to model the residual stresses caused by the temperature change and the restriction of movement of material due to the shrinkage and expansion of the elements in the mechanical modelling phase. After having the welding residual stress field obtained from this chapter, it will be used as an input for the new model for the cutting process in the next chapter.

3.1. Welding Simulation

The welding simulation analysis is a convenient method to distribute the residual stresses around the weld regions in welded components; although there is an uncertainty in the results compared to reality, it is a common tool to generate residual stresses. The welding simulation is performed to obtain stress results between the attachment and the base plate in the cruciform joint.

The welding simulation modelling is followed according to the MSc-thesis of N.J.H. van den Berg [24], since the same parameters for welding and material properties were used in this thesis. Certain assumptions were made to simplify the process, the results are not extremely accurate, but they do have a negative impact. The main assumptions and the modelling inaccuracies are the following:

- Only a quarter of the specimen is modelled. X and Y Symmetry conditions are used in the mechanical model to represent the other 3/4 of the cruciform specimen. This method completely mirrors the behaviour in the other directions making the welding process for all 4 weld seams to start at the same time, leaving no cooling time in between each weld seam. however, no symmetry conditions used in the the thermal model as it uses a "heat transfer analysis" which disallow the use of symmetry conditions, making the temperature flow in the model not mirrored to the other parts and giving an over-estimation of the heat effected zone due to only having half of the plate thicknesses modelled. This is explained more in depth in the results of the thermal model.
- Some mechanical boundary conditions applied to provide stability to the cruciform joint are over restricted. The deformation in the z-direction is over-restricted from one end, which means the FE model will over-estimate the welding induced residual stresses.
- There are no modelled material, geometrical, or welding flaws. weld flaws such slag inclusion and lack of penetration are disregarded. The FEM-material model's characteristics are continuous throughout the entire specimen.
- No weld penetration modelled; the plates and the weld are merged together in one part and have the same material properties for the steel S355 J2.
- The welding process is done in one pass only. One pass welding can only be used up to a certain thickness limit of 6.4 mm according to [25] and beyond this thickness, a multi-pass welding gives better results.

Geometry of the model

The dimensions of the model are shown in figure 3.1 and 3.2. As stated, only 1/4th of the cruciform joint is modelled on Abaqus FEA, and the other parts are not modelled but substituted with X and Y symmetry conditions. There is a gap between the vertical and the horizontal plates of 0.05 mm considered in the model to provide the realistic behaviour of the cruciform joint when loaded under tension. Avoiding modelling the gap in the numerical analysis could change the behaviour of the joint to be a non-loaded cruciform joint, which is not the case in this project.

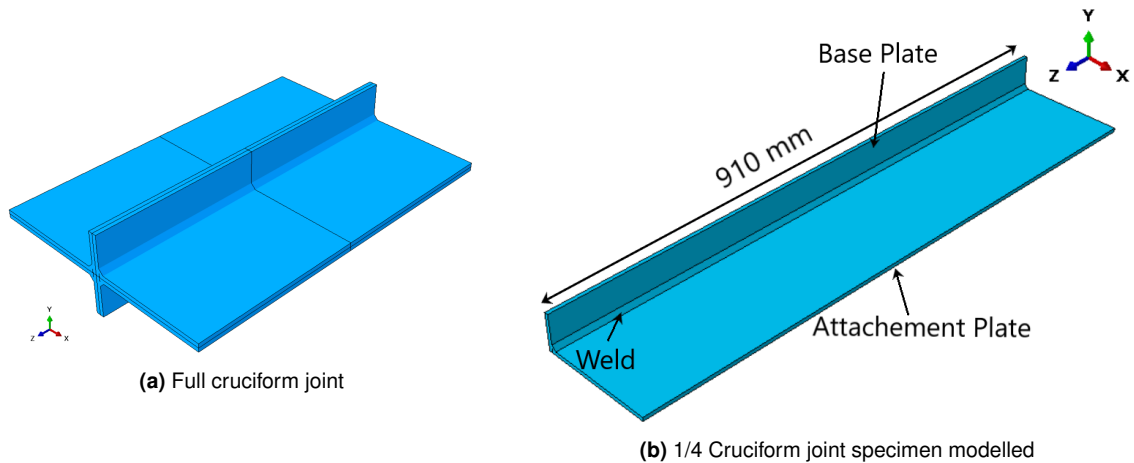


Figure 3.1: 1/4 cruciform joint model - simplification

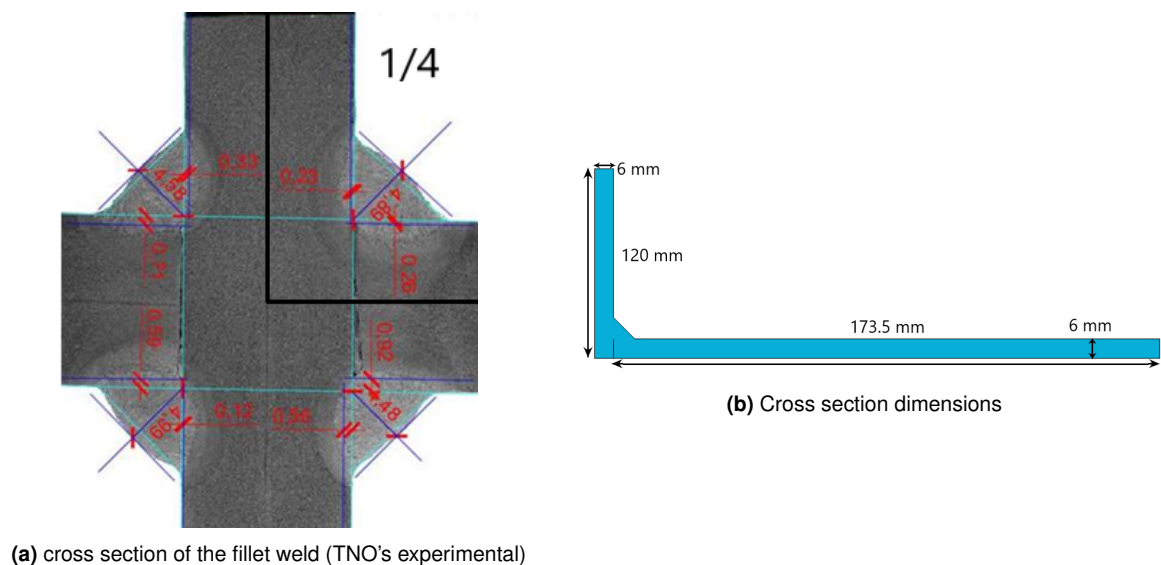


Figure 3.2: Cruciform joint cross section

3.1.1. Thermal model

The units for the heat input is presented in table 3.1. These properties are defined in the material properties in Abaqus, while other parameters were defined in the Interaction module by defining the radiation interaction using the "Surface radiation" which describes the heat transfer with a non-concave surface, and the "Surface film condition" which defines the heat transfer from surfaces due to convection.

Material properties

Steel S355 J2 is used for the cruciform joint specimen. Figure 3.3 shows the material properties according to NEN-EN-1993-1-2 and [24]. Figure 3.4 shows the stress-strain diagram per temperature. These properties are necessary for the weld simulation model.

Property	value	Unit
Length	910	mm
Density	7.85E-9	Tonne/mm ³
Temperature	-273.15	K
Conductivity	53.33	mW/mm.K
Specific Heat	4.70E8	mJ/tonne.K
Convection	0.01	mW/mm ² .K
Emissivity	0.5	
Heat Flux	1	mW/mm ³
Energy	1000	mJ
Stegan-Boltzmann constant	5.67E-11	mW.mm ⁻² .K ⁴

Table 3.1: Unit heat input model

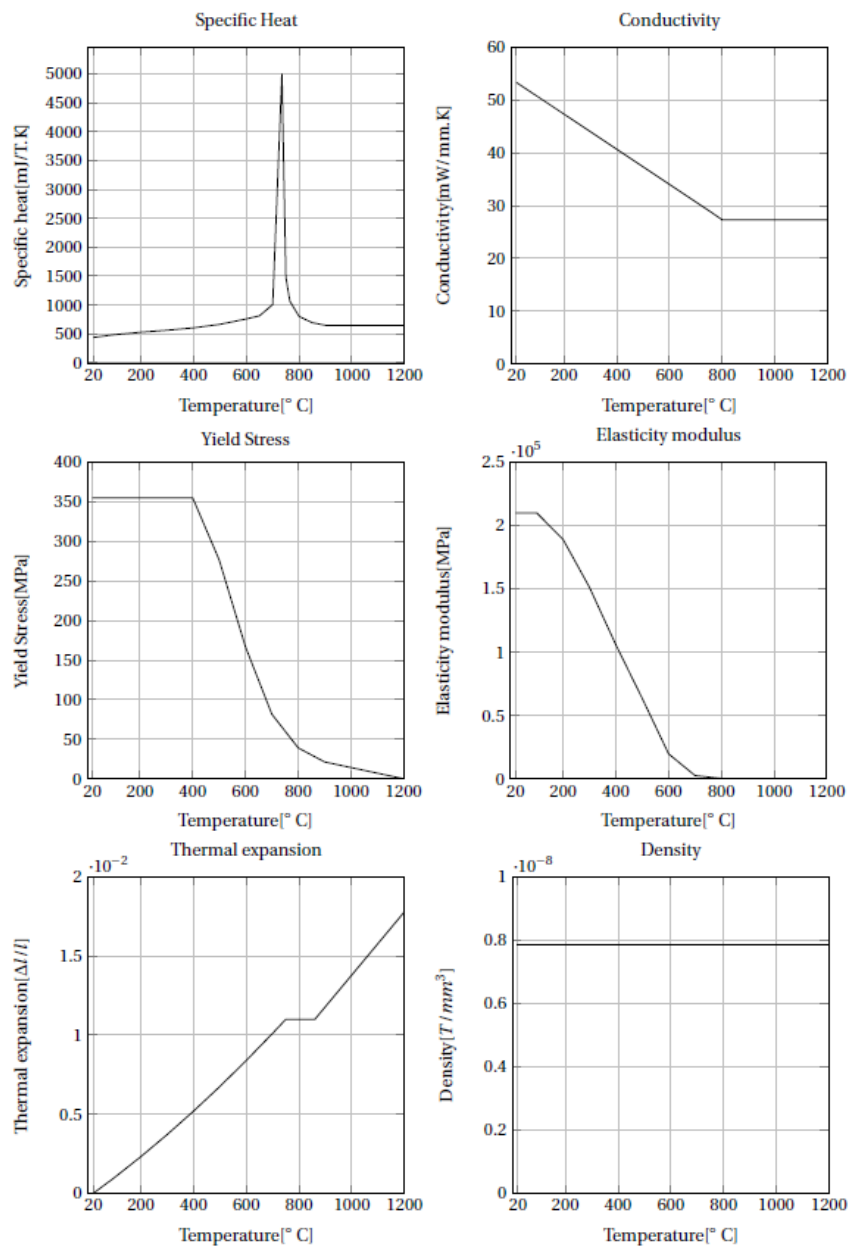


Figure 3.3: Material Properties

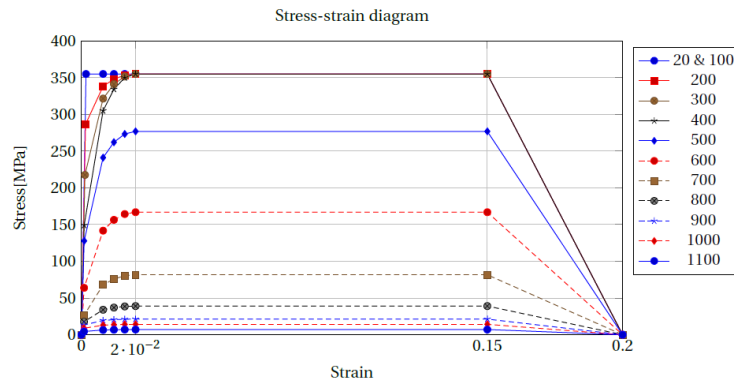


Figure 3.4: Stress-strain per temperature

Element activation

The element activation method is applied in both the thermal and the mechanical analysis. The process starts by having no material between the attachment and the base plate. The total weld is divided into 10 different element sets in Abaqus, each set has a length of 91 mm. The simulation starts with the first step called "Pre-step" in the analysis by having the weld component deactivated by using the interaction command in Abaqus called "model change" which allows the activation/deactivation of geometry or elements in the desired step. Once the total elements along the weld length are deactivated in the pre-step, the process at this point results in 'death' of the weld elements and the thermal analysis starts. As analysis proceeds, more time steps are completed, and with each step weld elements are reactivated; this process results in the 'birth' of weld elements. There are many elements in the weld region due to the fine mesh, so a python code was created to automatically select a specific number of elements and place them in an element set with a length of 91 mm; the python code is done for both the thermal and the mechanical model and are shown in Annex B. Figure 3.5 shows the elements highlighted in different colours.

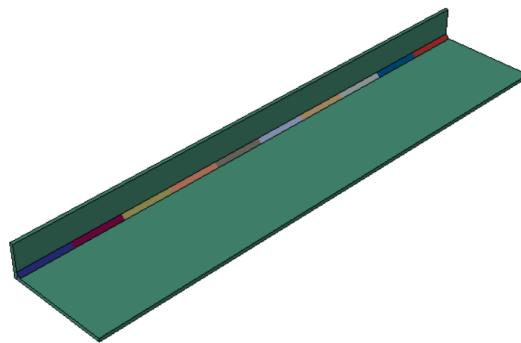


Figure 3.5: 10 element sets along the length of the weld

Welding simulation

The welding simulation starts with the thermal analysis by modelling the temperature during the welding process. The temperature at each node is registered per time increment; therefore it is more accurate to have a fine mesh around the weld region since the temperature gradient is large. As the filler material is added between the attachment and the base plate, the applied heat source bond the filler material and the parent material. The thermal process can be divided into three parts: Heat input, heat transfer through the specimen and heat loss.

Equation 3.1 represents the thermal process:

$$c\rho \frac{\partial T}{\partial t} = k \left(\frac{\partial^2 T}{\partial x^2} \right) + k \left(\frac{\partial^2 T}{\partial y^2} \right) + k \left(\frac{\partial^2 T}{\partial z^2} \right) + q \quad (3.1)$$

- T is the Temperature [Celsius]
- t is the time in seconds
- ρ is the density [T/mm^3]
- c is the specific heat capacity [$mJ/T.K$]
- q is the interal heat generation rate [mW/mm^3]
- k is the thermal conductivity [$mW/mm.K$]

The heat flux is modelled using FORTRAN subroutine called DFLUX within Abaqus and is presented in Annex A. This subroutine gives the input of the heat energy; it specifies the magnitudes time and the position of the welding within the model. The heat flux is calculated using two equations and by using the above parameters. The heat flux is modelled by the two ellipsoidal shapes [26] shown in figure 3.6, were there are two power density distributions for the from half ellipsoid and the rear ellipsoid.

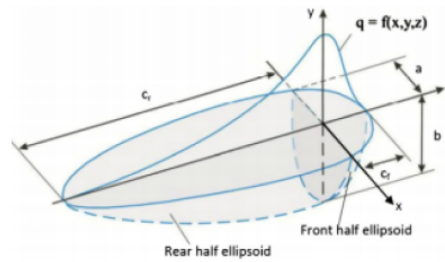


Figure 3.6: Heat source model [26]

The front power density distribution:

$$q_f(x, y, z) = \frac{6\sqrt{3}f_f Q}{abc_f \pi \sqrt{\pi}} e^{-3x^2/a^2} e^{-3y^2/b^2} e^{-3z^2/c_f^2} \quad (3.2)$$

The Rear power density distribution:

$$q_r(x, y, z) = \frac{6\sqrt{3}f_r Q}{abc_r \pi \sqrt{\pi}} e^{-3x^2/a^2} e^{-3y^2/b^2} e^{-3z^2/c_r^2} \quad (3.3)$$

the parameters are shown in figure 3.6

Table 3.2: Welding properties for the cruciform joint

Welding Properties		
Welding speed	10	mm/sec
Current	26	A
Voltage	600	V
Efficiency	0.95	
Heatflux	1.56E7	mJ/tonne.K
Width a	4.985	mm
Depth b	5	mm
Front c _f	4.985	mm
Back c _r	11.6	mm
Heat front f _f	0.7	
Heat back f _r	1.3	

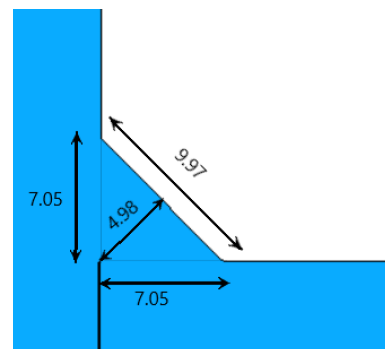


Figure 3.7: Weld dimensions

Mesh

DC3D8 (8-node linear heat transfer brick) elements with size 1.3 mm near the weld region were used in the thermal analysis. The mesh gets courses away from the weld region.

Results

The thermal model resulted in the temperature values at every time step over all parts of the joint. The steel weld melts at a temperature of 1200 degrees which is shown in the contour plot in grey.

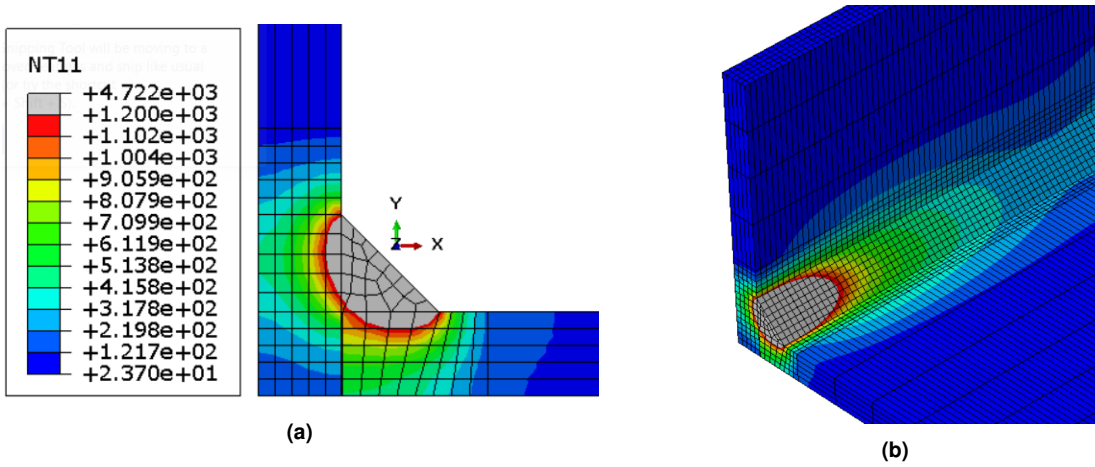


Figure 3.8: Heat model weld

A substantial difference in temperature is clear between the attachment and base plate near the gap region. A temperature of 23 Celsius at the bottom of the base plate (as seen in dark blue) when the temperature of the adjacent attachment plate is around 513 Celsius. This is considered as a modelling consequence and does not occur in real life welding processes. No effect of this will influence the results of the residual stresses at the bottom weld toe.

The type of analysis used in Abaqus FEA to model the thermal model is "heat transfer analysis" which was defined in the step analysis. Using the heat transfer analysis does not allow the setting of boundary or symmetry conditions, which means that there were no symmetry conditions applied in the thermal model to give the full behaviour of the cruciform joint, but the analysis is done for an L-shaped specimen.

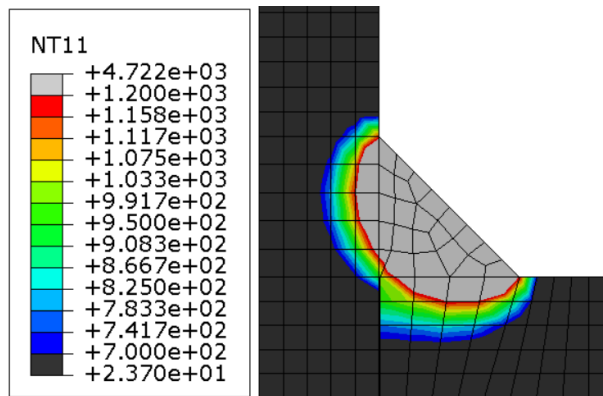


Figure 3.9: Heat affected zone

The results of temperature are effected in the plate areas. Not having the symmetry conditions applied on the back of the base and the attachment plates means that the heat transfer process in steel is different. Instead of having heat transfer within the steel material (thermal conduction), the heat is in fact being radiated to the surroundings. Which means that the temperature results at the base and attachment plates is not entirely correct, there should be more material for the heat to transfer to, but instead it radiates to the surroundings. Since the plates modelled as half the thickness (the 12 mm base and attachment plates are modelled here as 6 mm thickness), the heat affected zone size will be affected. The heat affected zone is a non-melted area of metal that has undergone changes in the material properties when exposed to high temperatures [27]. Steel S355 starts to have changes in the

material properties at around 700 - 800 Celsius as shown in figure 3.3. Thus, the heat affected zone in the temperature model can be estimated from figure 3.9. The grey area shows the area of the material under the melting point, while the different colors beyond that shows the heat affected zone and that a change in the micro-structure of the base and attachment plate undergo in terms of material properties. For such a thin plates and a relatively small size weld, the mesh size in this region is 1.3 mm and would give more accurate results to have more a finer mesh in this region for such thin plates.

It is more convenient to model the full geometry of the cruciform joint when analysing the heat affected zone when welding, since the thickness of the material is a major contributor of the heat affected zone. So, modelling of a the full cruciform joint geometry with a fine mesh around the weld region would generate an accurate size for the heat affected zone. This problem can be tackled by modelling a full and a quarter cruciform joint, and see what temperature differences occur.

3.1.2. Mechanical model

The temperature field from the thermal model is used as a predefined field in order to obtain the residual stress field due to welding process. Similar time steps as the thermal analysis are applied in the mechanical analysis with a similar sequence in terms of the "birth and death" principle. The generated stresses are formed due to the restrained deformations when expansion and shrinkage of the material. Elastic-plastic analysis is used in the mechanical model by defining temperature dependant elastic and plastic material properties.

Boundary conditions

The cruciform joint's boundary conditions have a significant impact on the stress distribution during the mechanical analysis. The joint is supported in each direction in order to provide stability of geometry when the weld elements are activated during the welding process. The over restriction of the deformation in the z-direction applied at the base and the attachment plates used in this welding simulation will generate higher residual stresses due the over constraint when the material is trying to contract when subjected to differences of temperature.

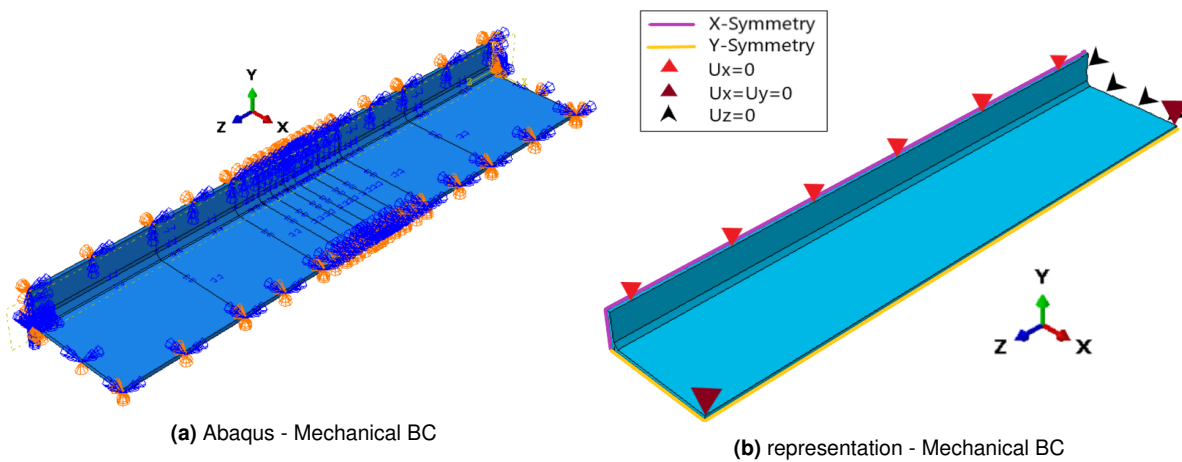


Figure 3.10: Mechanical Boundary Conditions

The expansion and contraction in the z-direction is not totally restricted, but should, to some limit, be stable to not cause distortions and movements while welding, so the right side of the base and attachments plates are set to $U_z = 0$. This one side restriction can cause some partial differences in residual stresses at the edges. If both sides were restricted, then higher residual stress would be generated. As indicated in figure 3.10, the attachment plate is entirely restricted in the y direction due to the y-symmetry condition, which gives a zero translation in the y direction $U_y = 0$. The x direction is only restricted at the end corners of the attachment plate, to avoid rigid body movement in the first weld increment activation but then to allow for some U_x movement in other parts of the attachment plate that may occur due to material shrinkage or expansion during heating and cooling. The base plate is restrained in the x-direction only which is provided by the x-symmetry condition, which gives a zero translation in the x direction $U_x = 0$.

After the welding process and cooling for 3500 seconds, all boundary conditions except the symmetry conditions are deactivated from the model and the results of residual stresses are recorded. The removal of boundary conditions corresponds to ramp down the reaction forces which are developed from the previous steps by changes of 7% in longitudinal tensile stresses at the centre of the weld toe ($Z=455$ mm), the stress decreased down from $\sigma_z = 457$ MPa to $\sigma_z = 424$ MPa, and the longitudinal compressive stress at the ends has changed by increasing the compressive stresses. The maximum compressive stress at the fully clamped end has gone from $\sigma_z = -67$ to $\sigma_z = -194$ MPa, which is an absolute difference of 127 MPa, while the free end has increased in compressive stress by only 64 MPa by going from $\sigma_z = -51$ MPa to $\sigma_z = -115$ MPa. Figure 3.16 presented in the results section shows the relaxation of stress.

Mesh

Performing a welding simulation for a large geometry makes it more difficult and time consuming when using a very fine mesh. However, the mesh was refined near the Weld region with a size of 1.3 mm but a course mesh was used further from the weld with a size of 10 mm. An instant transition of mesh size 5 mm away from the weld toe was done which can have a partial negative effect on the results. Linear hexahedron C3D8R (8-node linear brick, reduced integration, hourglass control) elements were used for the weld and the plates. Total number of elements through out the whole geometry is 166374 elements, and is compatible to the number of elements in the thermal model.

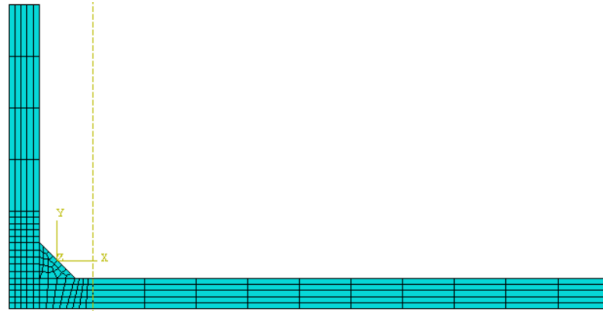


Figure 3.11: Mesh

Stress discontinuities

The birth of elements reactivates 10 weld increments, each with a length of 91 mm. As a consequence of reactivating the weld increments, stress discontinuities occur at the interface of each weld increment, causing higher tensile stresses and inaccuracy in stress distributions along the z-direction. The expansion of the elements due to the high heat and the simultaneous activation of the following weld element with a low temperature when the prior weld element is at its maximum temperature are the reason to result of the stress discontinuities. These stress discontinuities are a methodological error of this welding simulations, and hence can be ignored.

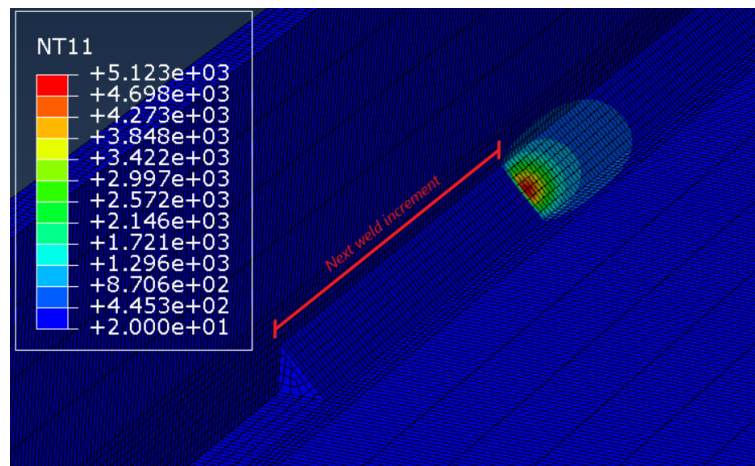


Figure 3.12: Temperature between weld increments

It can be seen in figure 3.12 that the temperature level at the end of the current increment is around 5120 degrees Celsius, while the temperature of the new weld increment is just 20 Celsius. The very high temperature of the weld increment is way above the melting point of the steel S355, which means that no matter what temperature above the melting point, the weld is in liquid state, thus the behaviour will almost be the same at this temperature range, but there will be faster conduction and radiation heat transfer with higher temperatures. The sudden temperature change causes these stress discontinuities.

There are several methods that can be done to minimise these stress distortions. Firstly, A finer mesh generally gives a higher accuracy in results but increases the computation time, so the mesh was

refined only around the weld region. secondly, a parameter called "Anneal temperature" was added to the material properties and set to a value of 1000 Celsius. Adding this parameter will change the behaviour of the plastic strain of the element by setting its value to zero when an element reaches a temperature of 1000 Celsius, and the material will be liquid-like material. As the temperature cools down and goes below 1000 Celsius, the plastic strain will have a non zero value again. This reduces the stress discontinuities, as a new weld increment is reactivated, the temperature of the activated weld increment is very high and due to the high temperature, the material will act as a liquid and will not generate stresses due to the re-activation of the new weld increment.

Results along the length of the weld toe show stress discontinuities, however for the sake of accurately monitoring the stress re-distribution after breaking down the specimen into smaller scale specimens, the stress results will be smoothed by taking the upper bound results as seen in figures 3.13 and 3.14.

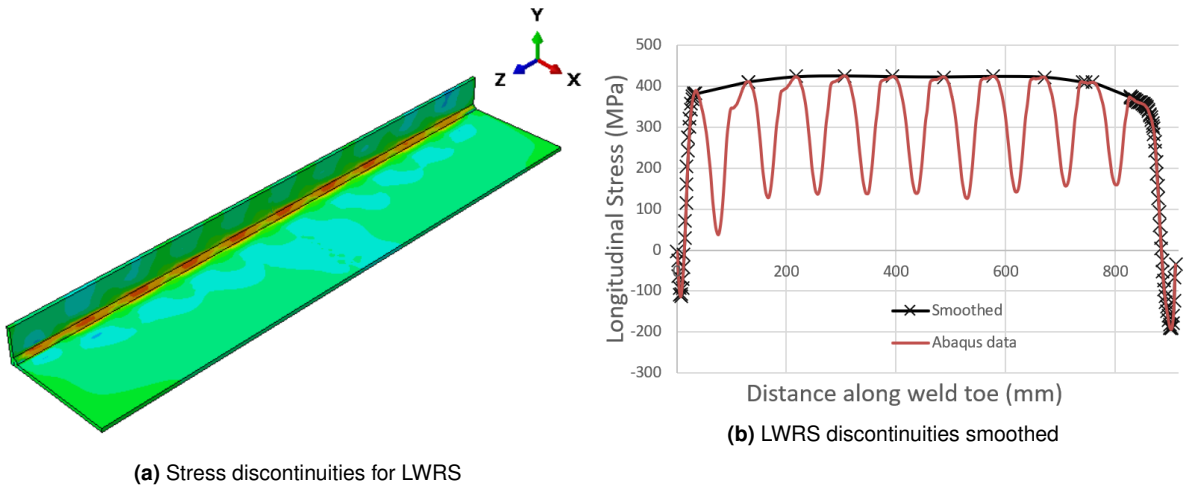


Figure 3.13: LWRS Stress discontinuities

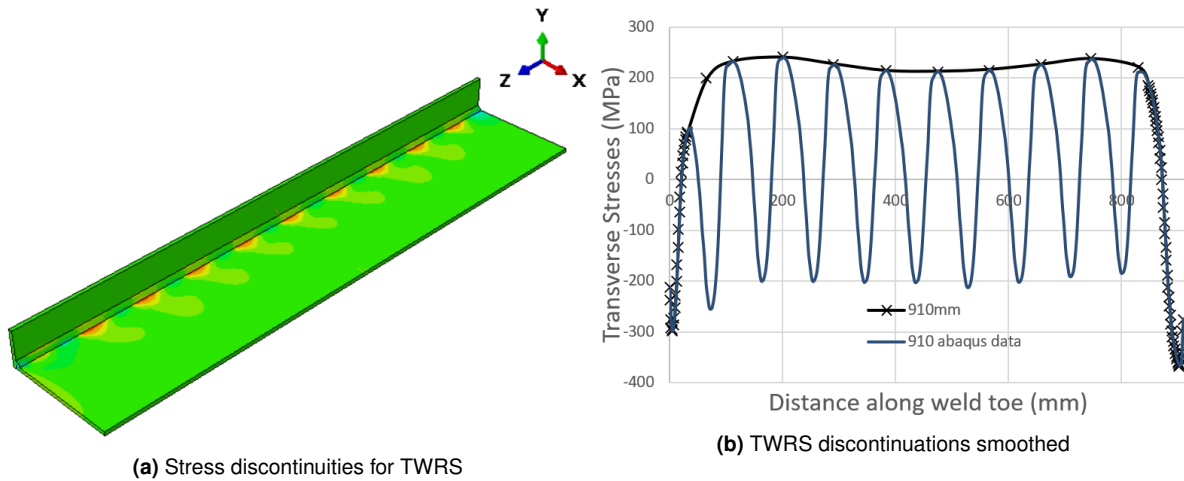


Figure 3.14: TWRS Stress discontinuities

Results

In this section, the longitudinal, transverse and maximum principle welding residual stresses along the weld toe line as highlighted in red in figure 3.15 (a) will be presented and discussed. The results are taken directly from the weld line, which is a place of a sharp transition with only a 1.3 mm element size. The stress levels directly at the weld toe are considered relatively higher than expected due to the singularity from the sharp transition between the weld and the attachment plate.

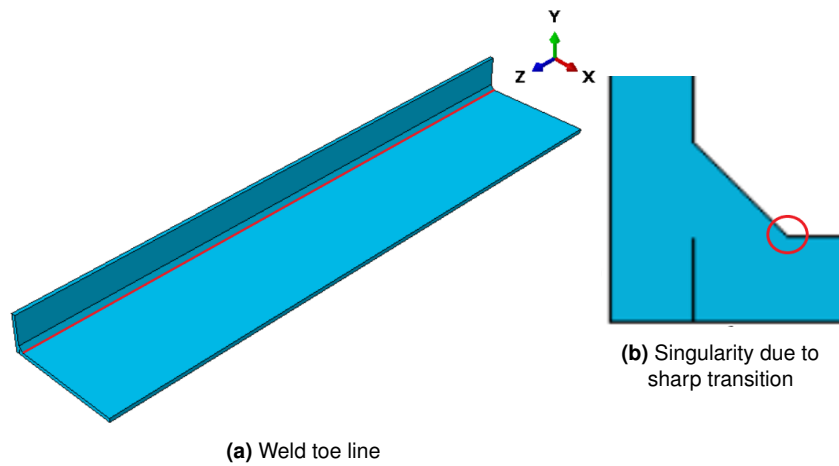


Figure 3.15

Firstly, the effect of the removal of the boundary conditions after the weld material has cooled down is presented in figure 3.16 and was discussed in earlier in the section.

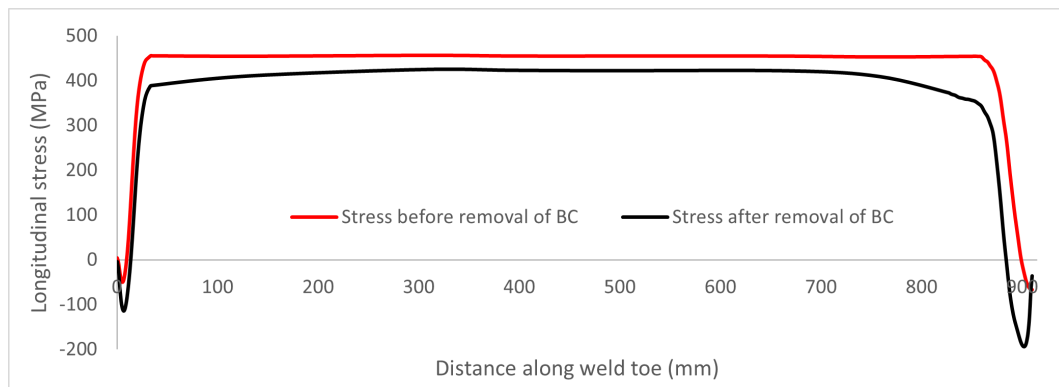
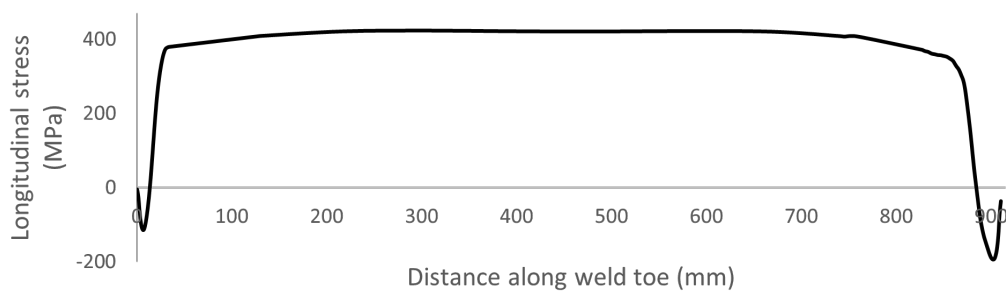


Figure 3.16: Longitudinal stress relaxation after BC removal

The stress results shown in figures 3.17 to 3.19 show a system of tensile and compressive which in total gives an equilibrium in the specimen. which means the large tensile stresses are balanced by compressive stresses in other parts. The longitudinal σ_z welding residual stress (LWRS) is the dominant stress compared to the transverse and maximum principle stress with a maximum tensile stress of 421 MPa at midpoint of $z=455\text{mm}$ as shown in figure 3.17 reaching a value higher the the yield stress of 355 MPa. Nearly a symmetrical behaviour on each end of the weld toe by having compressive stresses.

Figure 3.17: Longitudinal σ_z welding residual stress along weld toe

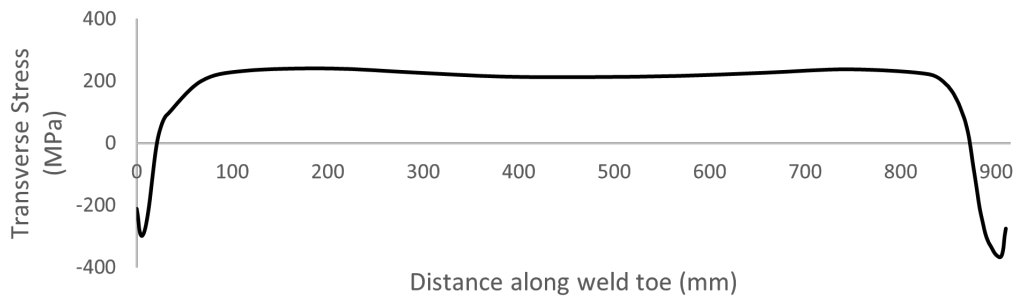


Figure 3.18: Transverse σ_x welding residual stress along weld toe

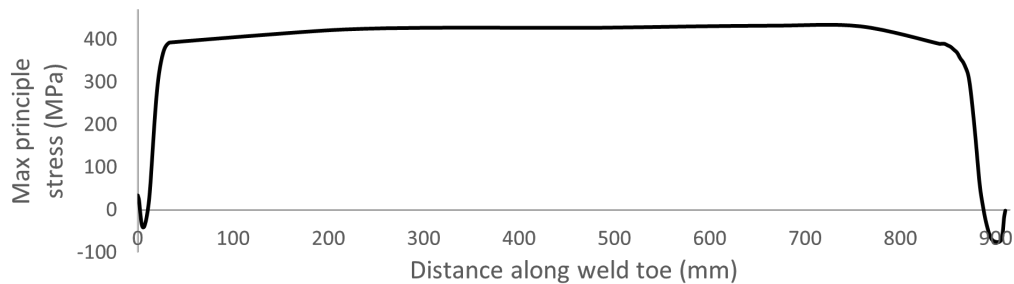


Figure 3.19: Maximum Principle welding residual stress along weld toe

The high stresses from the figures arise due to the fact that during the cooling process there was an extensive drop in temperature, the contraction and expansion of the material at the weld region is restrained by the adjacent material at lower temperature and due to the boundary conditions applied.

Effect of the over-constraint in the z-direction on one side

As can be seen in the compressive stresses that are on the right side (near the 910 mm edge) for the longitudinal, transverse, and maximum principle stresses as shown in figure 3.19 3.18 3.17. The peak compressive stresses where the plates are over-constrained are higher than the side where it is free to deform in the z-direction.

	Max compressive stress (MPa) at free end (no z BC)	Max compressive stress (MPa) at fully restricted end (near 910mm end)	Difference in MPa
Longitudinal (z) Stress	-114	-194	80
Transverse (x) Stress	-298	-367	69
Max. Principle Stress	-40	-75	35

Table 3.3: Maximum compressive stress comparison between weld ends

Table 3.3 shows the compressive stress at both ends of the weld seam after the removal of the boundary conditions. The peak compressive stresses at both ends with $U_z = 0$ and without $U_z = 0$ are shown in the table. It can be seen that restricting the deformation in the z-direction generates up to 47% higher residual compressive stresses. A peak longitudinal compressive stress of -194 MPa at the end where $U_z = 0$, while only a peak longitudinal compressive stress of -114 MPa at the end that can move freely in z, which gives a difference of 80 MPa. This shows the significance of the boundary conditions when performing a welding simulation.

4

Cutting of the full scale specimen

This chapter presents the cutting of the 910 mm long full scale cruciform joint into five small scale specimens using Abaqus FEA. An elasto-plastic analysis is performed using the same model with a consistent mesh as used in the welding simulation. The welding residual stress field obtained from the welding simulation is used as a predefined initial stress field and the redistribution of stress after cutting into smaller specimens is analysed and discussed. After generating multiple specimens, a load of 186.2 is set in the x direction and the stress levels at the weld toe is investigated. The same procedure is repeated but excluding welding residual stresses in the specimens to examine the contribution welding residual stresses for fatigue performance. The models excluding WRS are validated using 2D plane strain and plane stress models. The methodology of this chapter is summarised in the flowchart below 4.1.

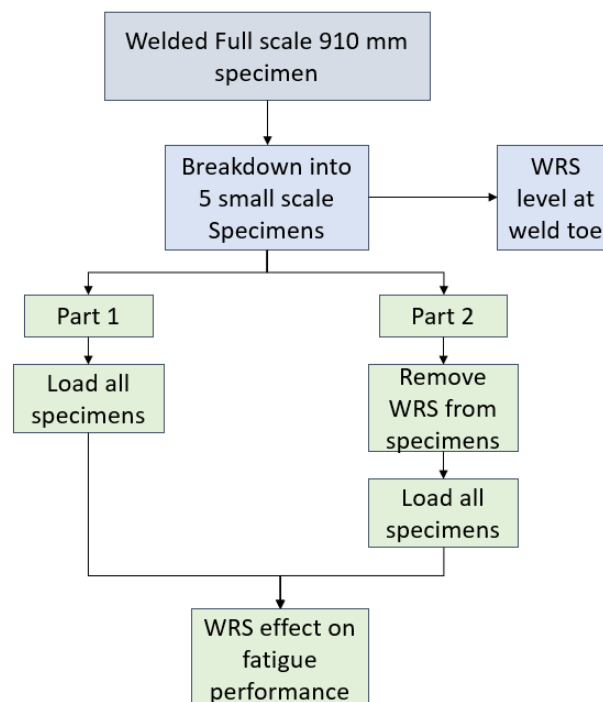


Figure 4.1: Chapter 4 flowchart

4.1. FE model for the cutting process

The data in the papers of [28, 29, 30, 31, 32] indicate that the residual stress level due to cutting is ignored since it only exists in a depth of 150-200 μm of the material. Hence, this process is only

considered as a stress relaxation process caused by the removal of the material; No deformation or residual stress due to cutting is considered. The cutting of the cruciform specimen was done by removing parts from both sides using the "Interaction - Model Change - Geometry deactivation" feature.


Length (mm)	Restart Step	Analysis	Task
910	 Step 1- Add the residual stress field generated from the welding simulation as a predefined initial stress field to the 910 mm long model.	1a	Load 910 mm specimen
500		2a	Cut 910 mm to 500 mm
		2b	Load 500 mm specimen
210		3a	Cut 910 mm to 210 mm
		3b	Load 210mm specimen
120		4a	Cut 910 mm to 120 mm
		4b	Load 120 mm specimen
75		5a	Cut 910 mm to 75 mm
		5b	Load 75 mm specimen
20		6a	Cut 910 mm to 20 mm
		6b	Load 20 mm specimen

Figure 4.2: Abaqus restart analysis

A restart analysis is used in Abaqus to repeat the step of cutting from the 910 mm specimen. After the full specimen is cut to 500mm, a restart analysis is done to go one step back and cut the 910mm specimen into 210mm and etc, which means that all the specimens are directly cut down from the 910 mm full scale specimen. The cutting process is summarised in figures 4.2.

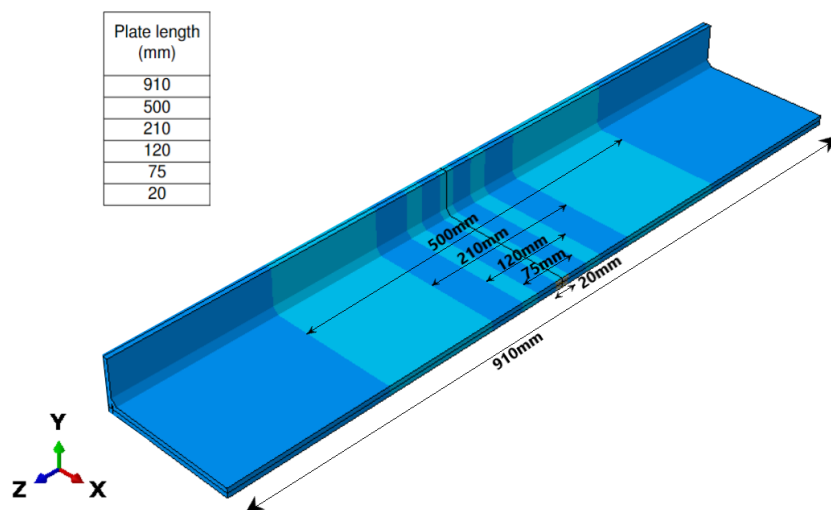


Figure 4.3: Schematic of the 910 mm long specimen step-by-step cutting process

4.1.1. Cutting Process Boundary conditions

In the actual execution of the cutting process, the specimen is required to be held through out the whole process. It is important to apply the appropriate boundary conditions to eliminate any rigid body displacement of the model.

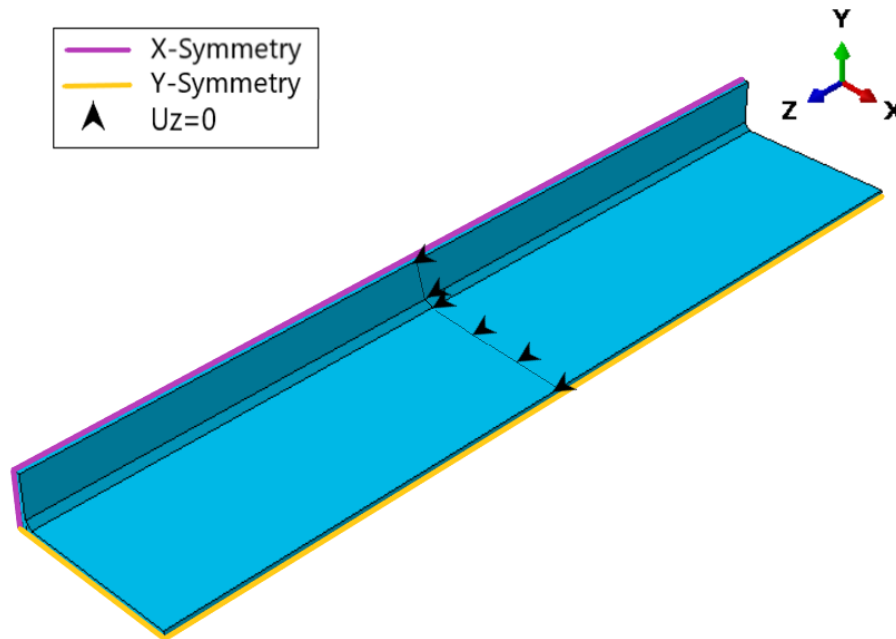


Figure 4.4: Boundary conditions representation for the cutting process

The X and Y symmetry conditions ($U_x=0$ and $U_y=0$) and restrict the displacement in the X and Y directions. The rigid body displacement in the Z direction is restricted along the mid-section at $z=455$ mm. This boundary condition is set in this location to not get deactivated in the part removal process as described in figure 4.2.

4.2. Welding residual stress evolution

4.2.1. Longitudinal WRS evolution

As seen in the results of the welding simulation, the dominant stresses for the 910 mm full scale specimen are the longitudinal WRS with a maximum tensile value of 421 MPa. Figures 4.5 to 4.10 show the LWRS after the cutting process. The evolution of the LWRS due to cutting at the weld toe is depicted in figure 4.11. The maximum tensile values of the LWRS for the different lengths of 910, 500, 210, 120, 75 and 20 mm occurs in the midsection at $z=455$ mm with values of 421, 402, 335, 271, 184 and 15 MPa, respectively. The peak compressive stress does not occur on the far end points of the weld, but close to the edges. The maximum compressive stress from 910 to 20 mm are -194, -138, -135, -41, -31 and -4 MPa respectively. Table 4.1 gives the maximum tensile and compressive LWRS along the weld toe for different specimen lengths.

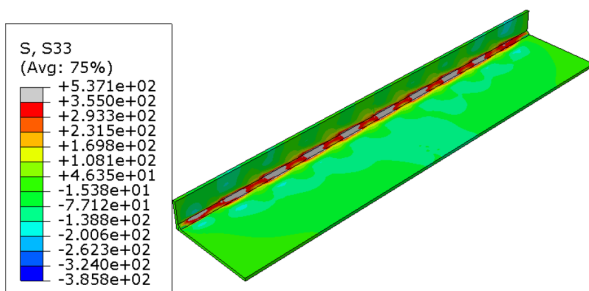


Figure 4.5: Full scale 910 mm

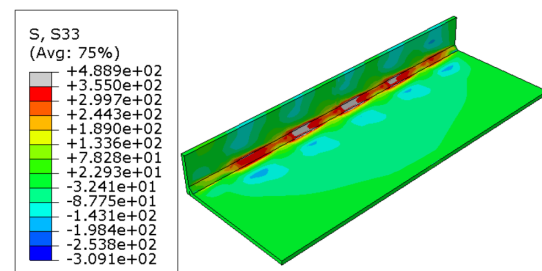


Figure 4.6: Small scale 500 mm

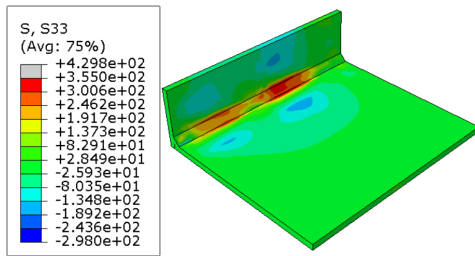


Figure 4.7: Small scale 210 mm

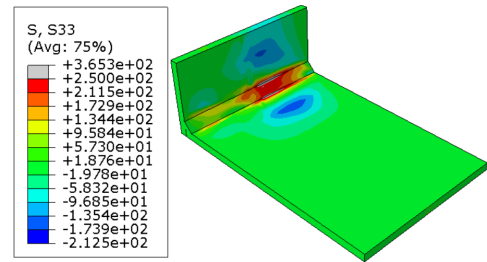


Figure 4.8: Small scale 120 mm

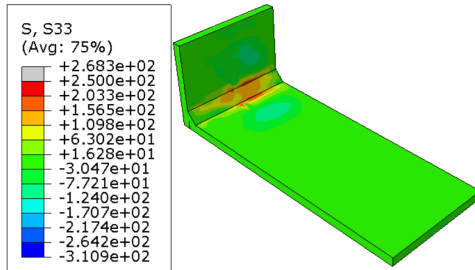


Figure 4.9: Small scale 75 mm

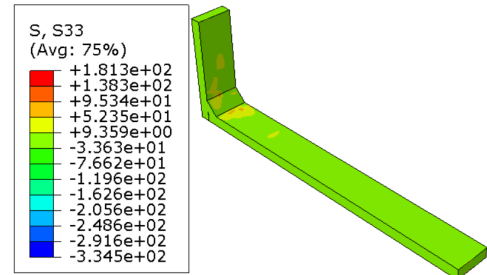


Figure 4.10: Small scale 20 mm

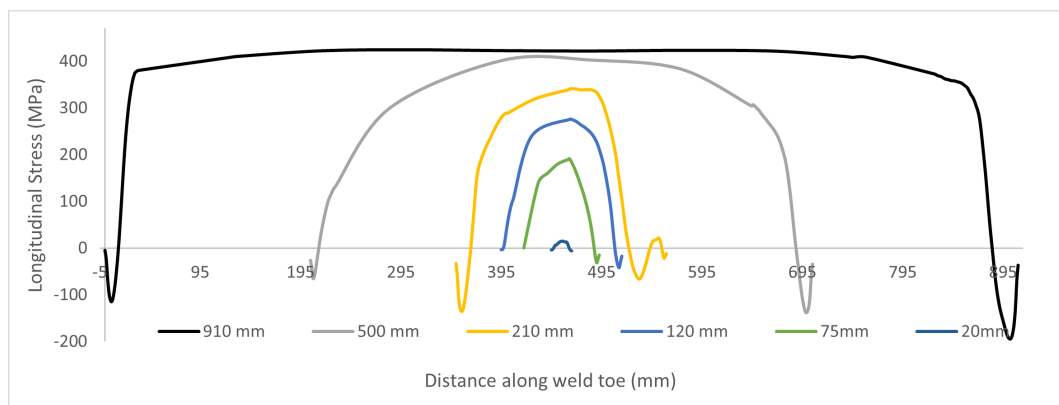


Figure 4.11: Evolution of LWRS due to cutting

A decrease of 406 MPa in tensile stress when cutting a full scale 910 mm long cruciform joint into 20 mm which is an immense change of approximately 96% and the relaxation of compressive stress however is approximately 98%. This indicates that 97% of the stresses from the 910 mm specimen are lost when cutting to a 20 mm long specimen, making it nearly free of LWRS. The 20 mm would give a higher fatigue life when assessed, due to having less tensile stresses and would include in reality less defects in the weld since the 20 mm represents only 2.2% out of the 910 mm length.

When the 910 mm was cut into 75 mm, the tensile stress level decreased from 421 to 184 MPa, a difference of 238 MPa which is a change of approximately 56% of peak tensile stresses, and a 84% change of maximum compressive stress. Table 4.2 summarises the loss of longitudinal tensile and compressive stresses when cut from 910 mm full specimen.

Specimen Length	Tensile stress (MPa) at z=455mm	Peak compressive stress (MPa)
910	421	-194
500	402	-138
210	355	-135
120	271	-41
75	184	-31
20	15	-4

Table 4.1: Maximum longitudinal tensile and compressive stresses along weld toe

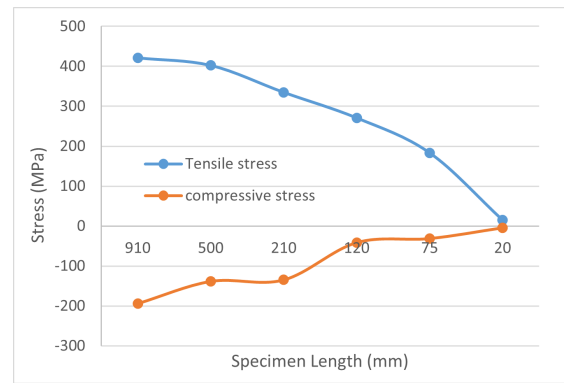


Figure 4.12: Decreasing trend of LWRS

Initial to final cut	Tensile stress loss (MPa) at z=455 mm	Change (%)	Compressive stress loss (MPa) along z	Change (%)
910 to 500	19	5	56	29
910 to 210	86	21	59	31
910 to 120	150	36	153	79
910 to 75	238	56	163	84
910 to 20	406	96	190	98

Table 4.2: Longitudinal stress loss from full scale to small scale specimen comparison

29% of compressive stress relief near the ends and 5% tensile stress change when going from 910 to 500 mm. The tensile stresses are undesirable when it comes to fatigue, and in this case a small change occur which means that the 500 mm specimen has almost the same fatigue performance when being assessed in terms of number of cycles only under the assumption that the weld seam is free of defects. In reality the fatigue performance is somehow different due to the presence of extra defects in the weld when the specimen is longer.

4.2.2. Transverse WRS evolution

The transverse welding residual stresses obtained from the welding simulation show a lower stress levels compared to the longitudinal WRS. The peak tensile stress did not occur at the midsection ($z=455$ mm) but occurred at 202 mm with a value of 240 MPa. Figures 4.43 to 4.48 show the TWRS after the cutting process. The evolution of the TWRS due to cutting at the weld toe is summarised in figure 4.19.

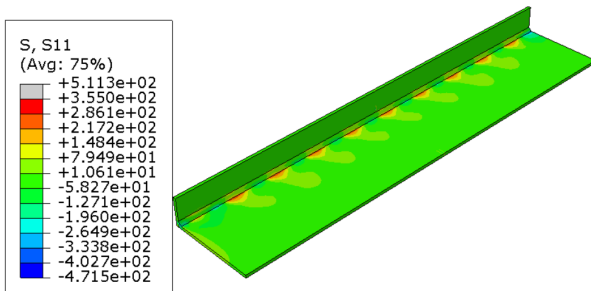


Figure 4.13: Full scale 910 mm

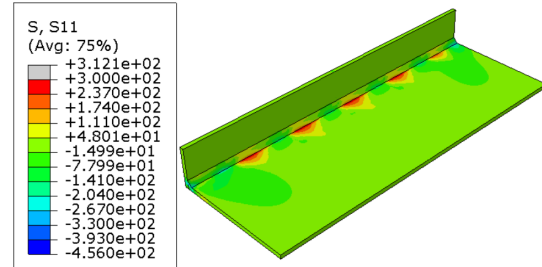


Figure 4.14: Small scale 500 mm

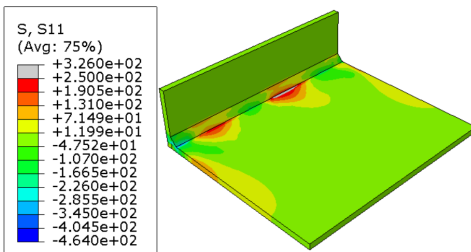


Figure 4.15: Small scale 210 mm

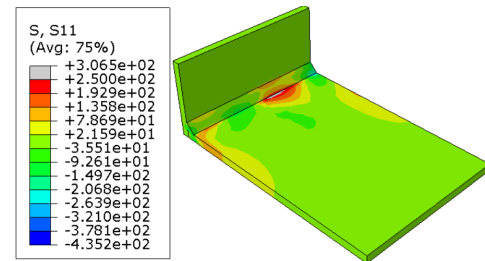


Figure 4.16: Small scale 120 mm

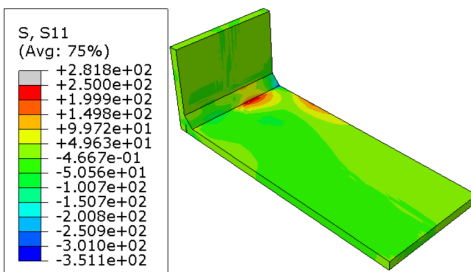


Figure 4.17: Small scale 75 mm

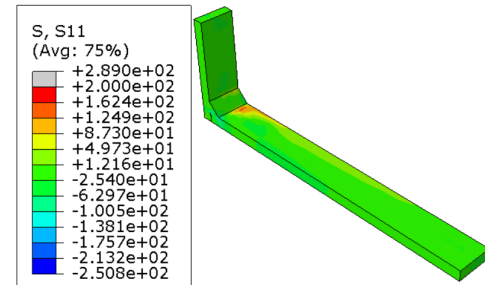


Figure 4.18: Small scale 20 mm

Table 4.4 and 4.3 summarises the tensile and compressive TWRS along the weld toe for all specimen lengths and the transverse stress loss when cutting from 910 mm to a small scale specimen.

The trend for the transverse tensile welding residual stress is completely different compared to the longitudinal WRS. The maximum tensile TWRS occurred in the midsection of the specimen for the 210 mm specimen with a value of 259 MPa. The 500, 210, 120 and 70 mm all show a slightly higher value of tensile transverse stress than the full scale 910 specimen in the midsection, except the 20 mm which is 81% less than 910 mm specimen value.

The 20 mm again shows a tremendous stress level difference when cut from the 910 mm specimen; the max tensile and compressive stress for the 20 mm specimen is 40 and -77, respectively, giving a substantial difference in terms of fatigue performance. From the TWRS and the LWRS results, it can be concluded that a 20 mm small scale cruciform joint specimen does not give valid results when tested for fatigue due to the large difference of WRS at the weld toe.

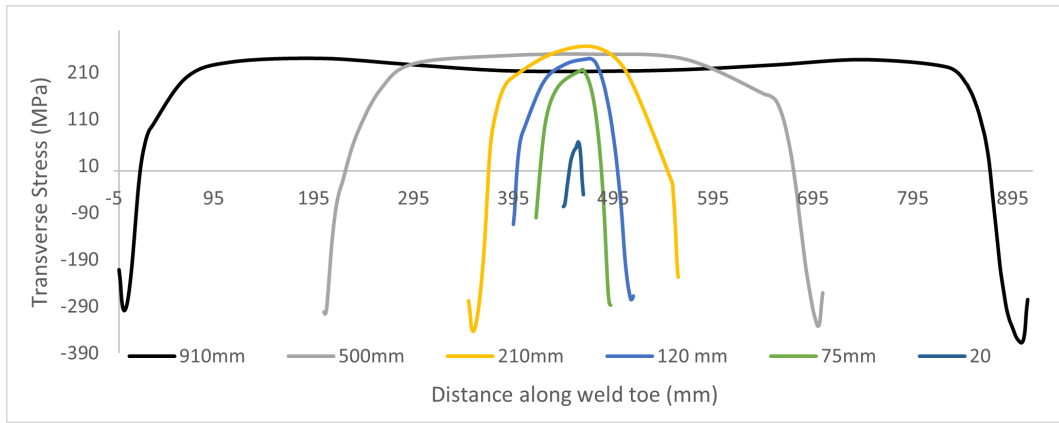


Figure 4.19: Evolution of TWRS due to cutting

Specimen Length	Tensile stress (MPa) at z=455mm	Peak compressive stress (MPa)
910	213	-367
500	248	-332
210	259	-342
120	234	-274
75	216	-287
20	40	-77

Table 4.3: Maximum Transverse tensile and compressive stresses along weld toe

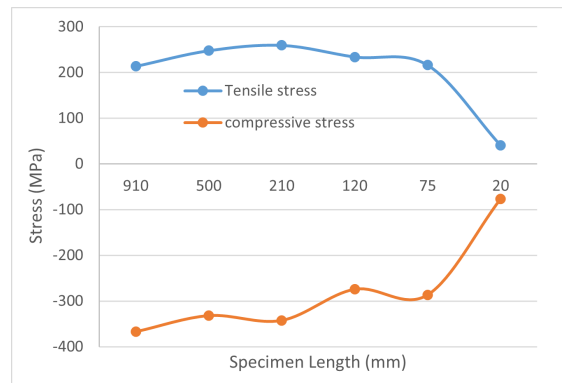


Figure 4.20: Trend of TWRS

Initial to final cut	Tensile stress loss (MPa) at z=455 mm	Change (%)	Compressive stress loss (MPa) along z	Change (%)
910 to 500	19	16	10	35
910 to 210	-46	22	7	25
910 to 120	-21	10	25	93
910 to 75	9	4	22	81
910 to 20	173	81	79	290

Table 4.4: Transverse stress loss from full scale to small scale specimen comparison

4.2.3. Max Principle stress evolution

The maximum principle stress is an important factor for inspecting the largest tensile and compressive flow directions at a zero shear stress. It is vital when assessing fatigue performance and fracture of materials since the crack will propagate perpendicular to the largest principle stress range. As can be seen from the figures, especially figure 4.27 that is giving a compatible trend of stress evolution due to cutting to the longitudinal welding residual stresses, and that was in fact expected because the LWRS are the dominant stresses compared to the TWRS.

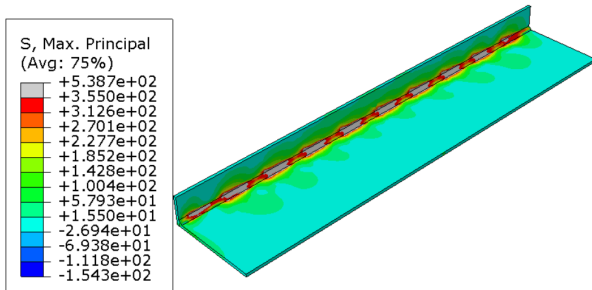


Figure 4.21: Full scale 910 mm

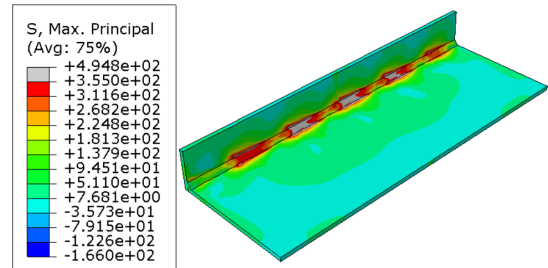


Figure 4.22: Small scale 500 mm

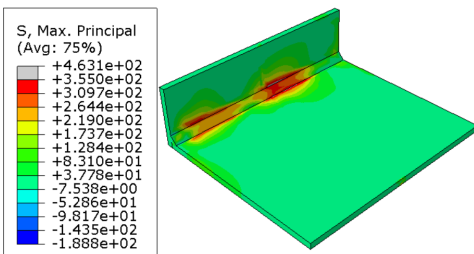


Figure 4.23: Small scale 210 mm

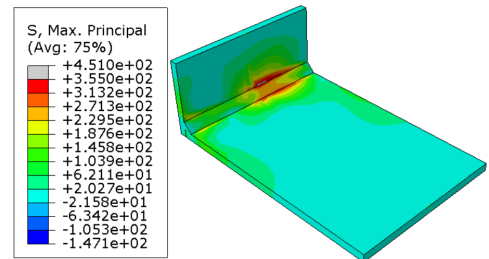


Figure 4.24: Small scale 120 mm

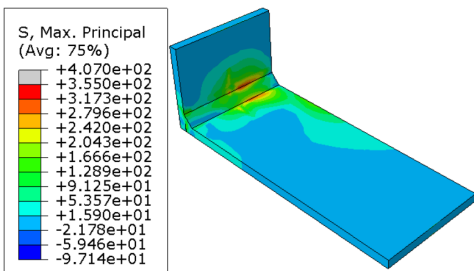


Figure 4.25: Small scale 75 mm

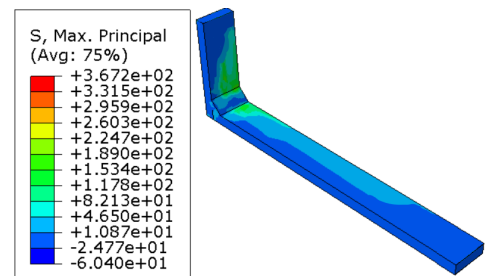


Figure 4.26: Small scale 20 mm

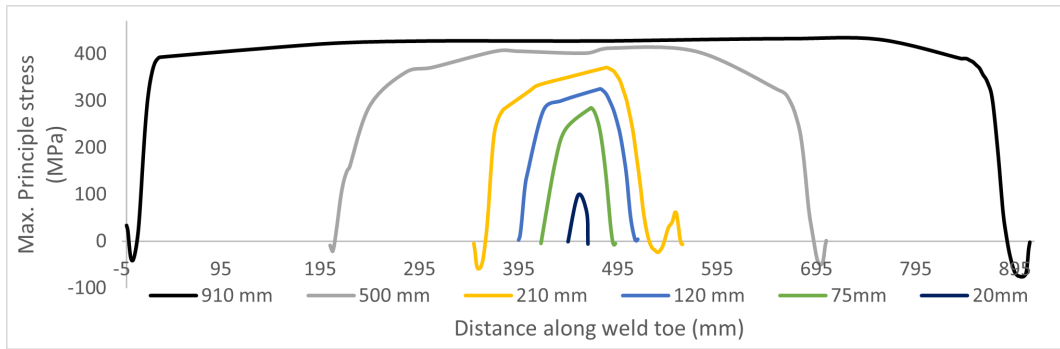


Figure 4.27: Evolution of Max. Principle stress due to cutting

Specimen Length	Tensile stress (MPa) at z=455mm	Peak Compressive Stress (MPa)
910	427	-76
500	403	-50
210	358	-58
120	312	3
75	268	-5
20	98	-6

Table 4.5: Maximum Principle tensile and compressive stresses along weld toe

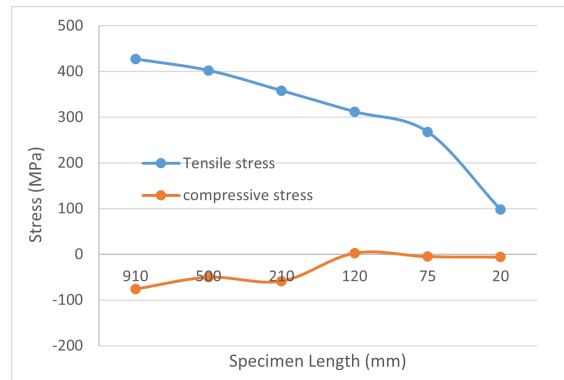


Figure 4.28: Decreasing trend of Max principle WRS

Initial to final cut	Tensile stress (MPa) at z=455mm	Change (%)	Compressive Stress loss (MPa) along z	Change (%)
910 to 500	25	6	26	34
910 to 210	69	16	17	23
910 to 120	115	27	78	103
910 to 75	159	37	71	93
910 to 20	329	77	70	92

Table 4.6: Maximum Principle stress loss from full scale to small scale specimen comparison

4.3. Loading of welded specimens

This section presents the longitudinal, transverse and maximum principle stresses and the results of each are divided into two parts. Firstly, all specimens **including WRS** are set under a tension load of 186.2 MPa from the edge of the attachment plate in the x direction as shown in figure 4.29, and the redistribution of WRS after loading at the weld toe is presented. Secondly, the same procedure is done to the specimens but the **WRS are excluded**; only the stress due to loading is presented. The effect of WRS is analysed based on the difference in the stress levels between part the two parts.

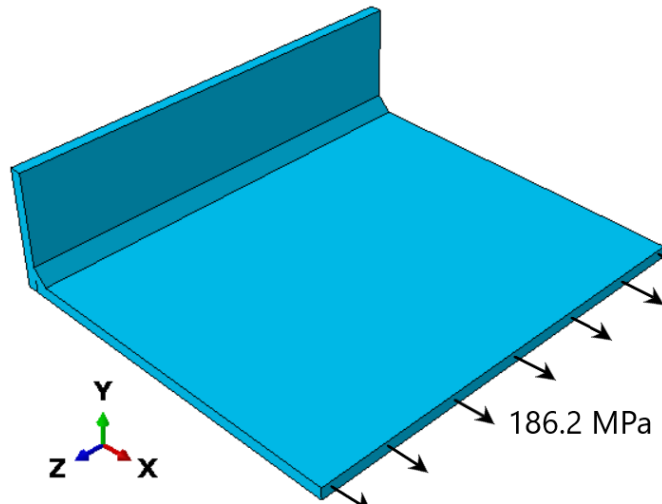


Figure 4.29: Tension loading

Fatigue loading is set to have a maximum and a minimum value with their difference defined as the stress range which goes in cycles. A stress range of 93.1 MPa was used to test the cruciform joint for fatigue, with a stress ratio of 0.5 to give a maximum stress of 186.2 MPa and a minimum stress of 93.1 MPa. The maximum tensile stress of 186.2 is used in the analysis.

4.3.1. Longitudinal Stress

The results of the longitudinal stress at the weld toe due to loading+WRS and due to loading only are presented and discussed below.

Stress due to Load and WRS

Figure 4.36 and 4.37 show in dashed line the redistribution of the stress due to welding after loading.

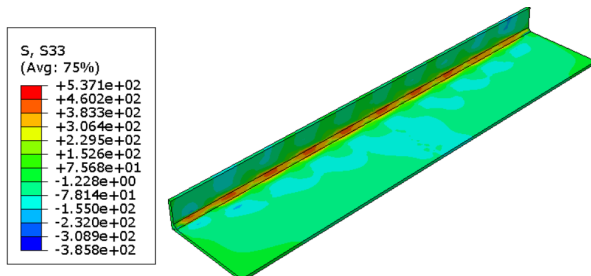


Figure 4.30: Full scale 910 mm

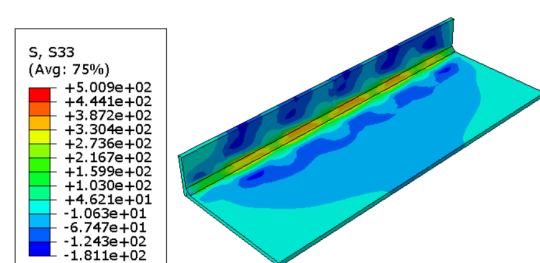


Figure 4.31: Small scale 500 mm

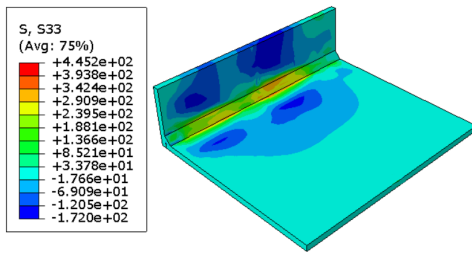


Figure 4.32: Small scale 210 mm

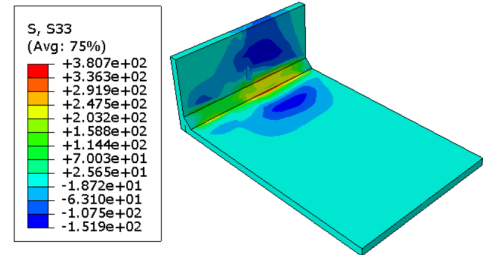


Figure 4.33: Small scale 120 mm

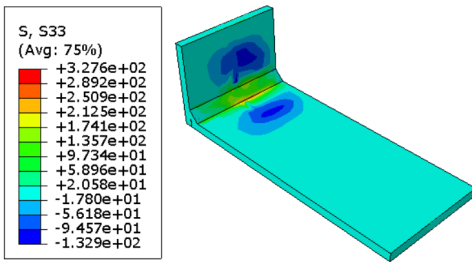


Figure 4.34: Small scale 75 mm

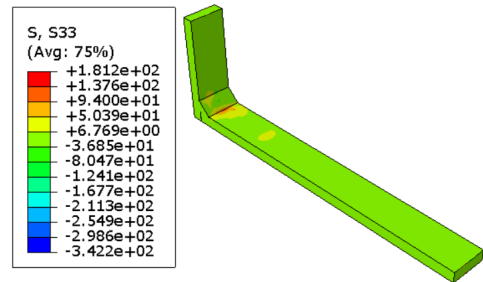


Figure 4.35: Small scale 20 mm

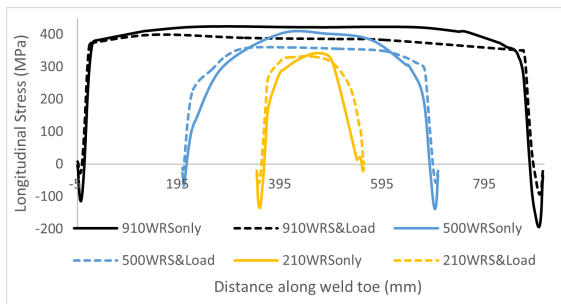


Figure 4.36: WRS vs. WRS and Loading for 910, 500 and 210 mm

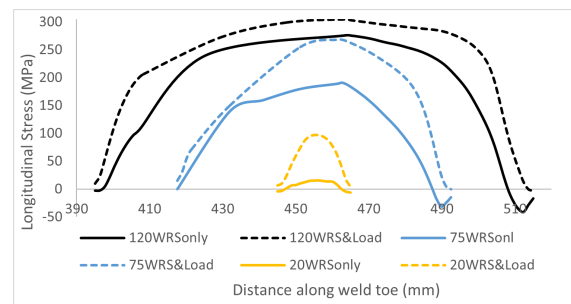


Figure 4.37: WRS vs. WRS and Loading for 120, 75 and 20 mm

As the loading is applied, a reduction in tensile and compressive longitudinal stresses occur for the 910, 500 and the 210 mm specimens, but an increase in stress in tensile stress for the 120, 75 and 20 mm due to the planar dimension change influence under the 186.2 MPa load. The decrease of the length parameter changes the thickness to length ratio of the specimen, causing the behaviour to change from plate-like to a beam-like behaviour. The stress at the weld toe would then redistribute for the plate-like specimens, but increase in stress for the beam-like specimens due to have a less distributed and a more concentrated load.

For a stress to relax with great values, a complete cycle of fatigue load has to be set. In this case, the cruciform joint is set under the maximum value of load, which means that the stresses levels at the weld toe should increase and not relax. Indeed they do increase, however not for the long specimens of 910, 500 and 210 mm, and that is due to Poisson's effect. The specimens are loaded in the x direction, so for a long plate, the longitudinal tensile stresses would decrease due to having a higher deformation in z-direction for longer plates that exhibit plate-like behaviour as shown in figure 4.40, the more the deformation, the higher the longitudinal compressive stress applied due to poisson's effect. The poisson's effect for shorter specimens is not as effective and gives less deformation as seen in figure 4.39 for the 20 mm specimens because the load in x direction is so effective when applied to a beam-like body, so the axial force in x direction is almost concentrated in the x and not the z direction due to the difference in planar dimensions between the 910 mm and the 20 mm for example.

Stress due to Load only

The predefined initial stress field in this model has been deactivated to analyse the stress distribution due to load only. The results FE results are shown below and the longitudinal stress for each specimen is summarised in figure 4.38.

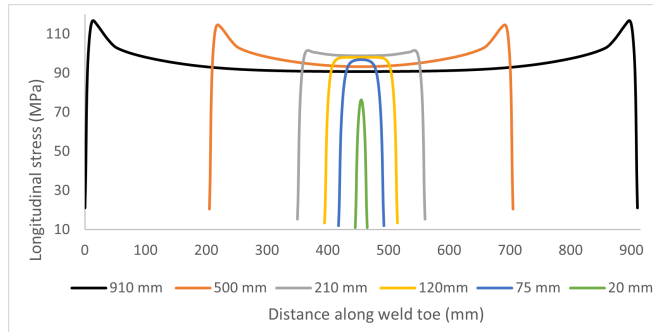


Figure 4.38: Longitudinal stress due to load only

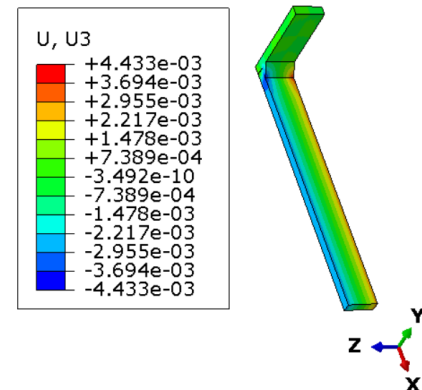


Figure 4.39: Deformation in z-direction for 20 mm specimen

Figure 4.38 indicates that the tensile longitudinal stress σ_z at the weld toe have peak stresses on the ends of the weld (at $z=0$ and $z=910$ mm) for the 910, 500 and 210 mm specimens. The peak stresses on the ends occur for multiple reasons, and mainly the restriction in contraction in the longitudinal z direction due to the high stiffness in the location caused by the presence of the base plate and the weld. When the load is applied transverse x -direction, the material should contract in the z -direction due to Poisson's effect as seen in figure 4.40.

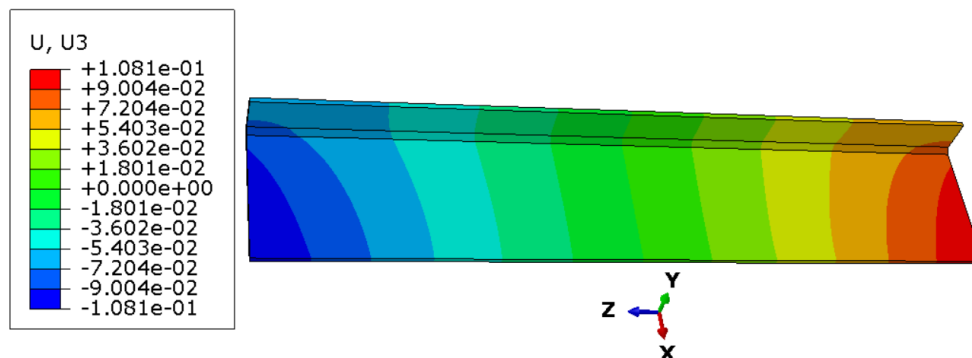


Figure 4.40: Deformation in z-direction for 910 mm specimen

Going from 910 to 20 mm, the length/thickness ratio increases significantly thus increasing the longitudinal deformation. The longitudinal deformation U_z when loaded in x -direction gives a zero displacement in the midsection as there are no geometrical imperfections assumed, but a displacement of 0.108 and 0.0044 mm for the 910 and 20 mm specimens, respectively.

Stress results including and excluding WRS

The results in this subsection proves the vitality of considering the impact of incorporating residual stresses when performing FE modelling. The dominant stresses from the numerical models are taken to be used in calculating the fatigue life in terms of number of cycles. Figures 4.41 and 4.42 show a major difference of stress at the weld toe when loaded with and without WRS.

The behaviour is almost completely different when comparing the dashed and solid lines in the graphs. For the 910, 500 and 210 mm, the peak stresses are found near the ends when no WRS included, but near the centre when including WRS in FE modelling. Thus, the prediction of the crack

initiation site which occurs at the locations of peak stresses would be completely different in this case. However, the peak stresses for 120, 75 and 20 mm specimens occur in the midsection for both, but still give a big difference in tensile stresses in the midsection except for the 20 mm specimen.

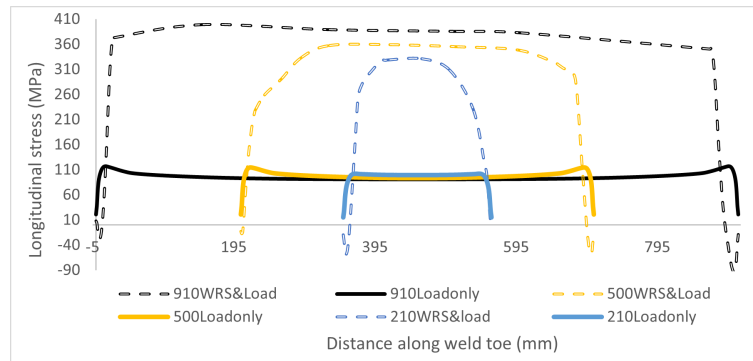


Figure 4.41: WRS & Load vs. Load only for (910, 500 and 210mm)

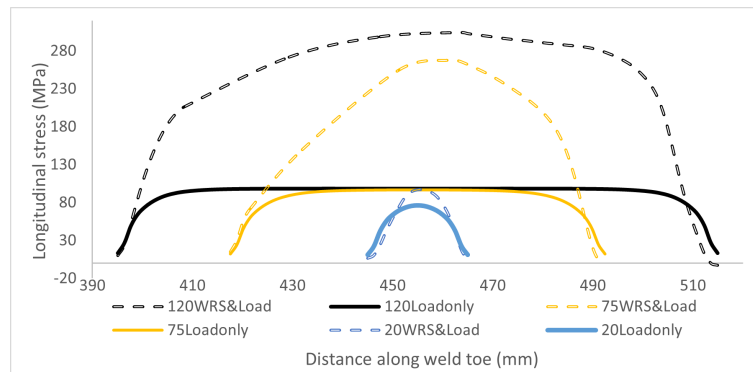


Figure 4.42: WRS & Load vs. Load only for (120, 75 and 20 mm)

Length (mm)	Max stress including LWRS (MPa)	Max stress excluding LWRS (MPa)	Difference in stress (MPa)
910	399	117	282
500	359	115	244
210	331	102	230
120	305	98	206
75	268	97	171
20	97	76	20

Table 4.7: Difference in peak stress when including and excluding LWRS in FEA

Only a difference of 20 MPa of peak stresses for the 20 mm specimen, which would not much change the fatigue life performance, and that is because the 20 mm is almost free of WRS due to its small size and enormous residual stress relief after cutting. So it can be concluded that it can be sufficient perform a numerical model without including a welding residual stress field to predict the fatigue life for a 20 mm specimen since the 20 mm specimen is almost free of WRS.

4.3.2. Transverse Stress

The results of the Transverse stress at the weld toe due to loading+WRS and due to loading only are presented and discussed below.

Stress due to Load and WRS

Figures 4.49 and 4.50 show in dashed lines the redistribution of the stress due to welding after loading. There is on average a 40% increase in transverse stresses and that is due to the fact that these stresses are also in the direction of the loading. The shape of the stress distribution has also flattened due to the load, causing the values of the transverse tensile stresses at the midsection to get closer as going from 910 to 20 mm, the maximum values are then 387, 390, 395, 397, 395 and 353 MPa, respectively.

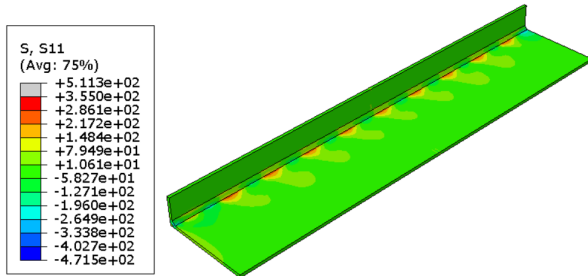


Figure 4.43: Full scale 910 mm

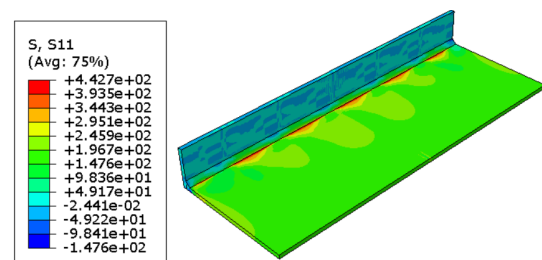


Figure 4.44: Small scale 500 mm

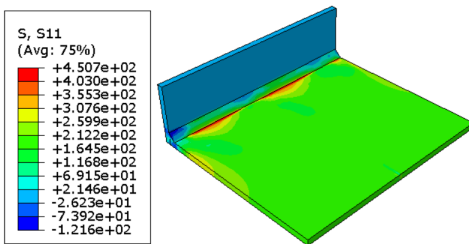


Figure 4.45: Small scale 210 mm

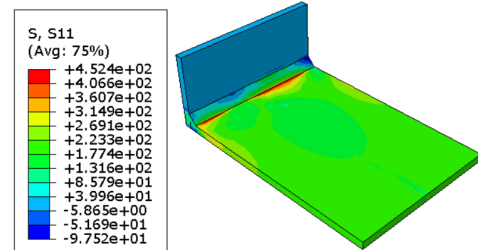


Figure 4.46: Small scale 120 mm

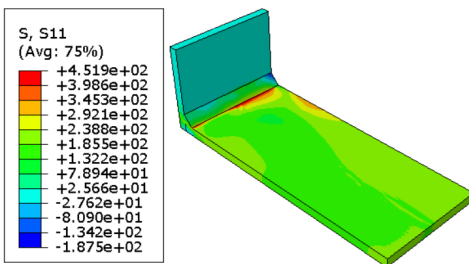


Figure 4.47: Small scale 75 mm

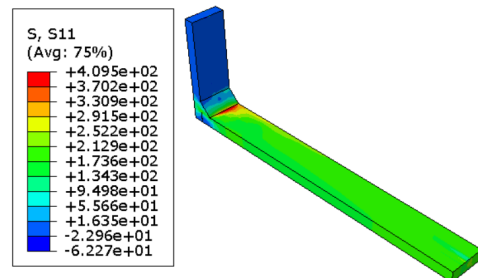


Figure 4.48: Small scale 20 mm

The transverse stresses due to load and welding combined gives stress values that are above the yield stress of 355 MPa, and are higher than the longitudinal stresses (due to load + welding combined), except for the 910 mm specimen as shown in table 4.8, which gives a slightly higher stress in longitudinal stress than the transverse stress.

As the 186.2 MPa load is applied in the x direction, it makes sense that the transverse stresses (in the x direction) to have a major increase. The applied tensile load also has also eliminated the compressive stresses on the edges of each specimen by making them tensile stresses with low values.

Length (mm)	Longitudinal stress (MPa) due to welding+Load	Transverse stress (MPa) due to welding+Load
910	399	387
500	359	390
210	331	395
120	305	397
75	268	395
20	97	353

Table 4.8: Longitudinal vs. Transverse stress due to load and welding

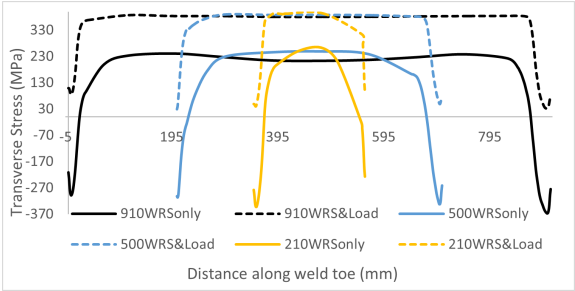


Figure 4.49: WRS vs. WRS and Loading for 910, 500 and 210 mm

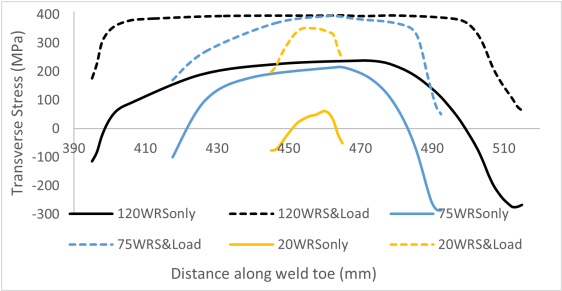


Figure 4.50: WRS vs. WRS and Loading for 120, 75 and 20 mm

Stress due to Load only

The predefined initial stress field in this model has been deactivated to analyse the stress distribution due to load only. The results FE results are shown below and the transverse stress for each specimen is summarised in figure 4.51

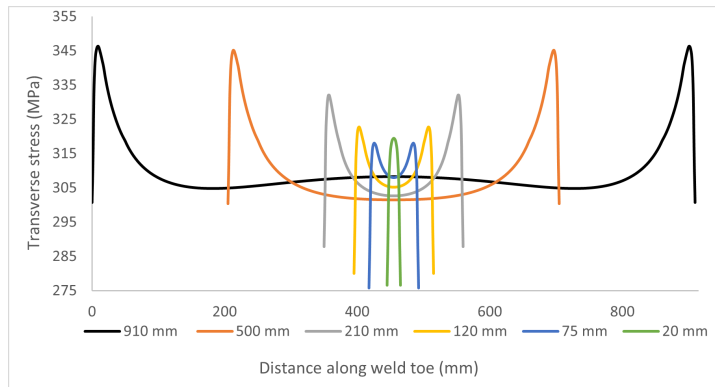


Figure 4.51: Transverse stress due to load only

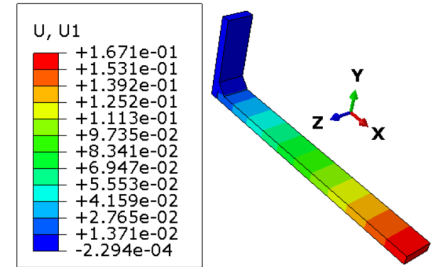


Figure 4.52: Deformation in x-direction for 20 mm specimen

The peak stresses occur in the ends of the weld toe line for all specimens except the 20 mm specimen, which has a peak transverse stress of 320 MPa in the centre at z=455mm.

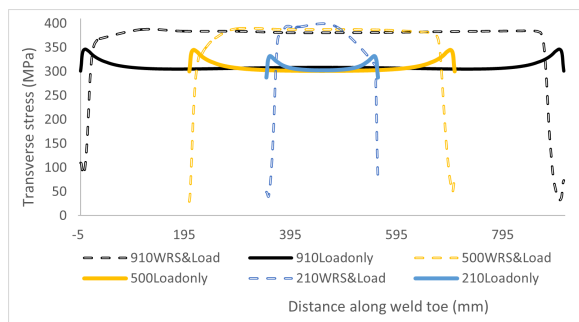


Figure 4.53: WRS & Load vs. Load only for (910, 500 and 210mm)

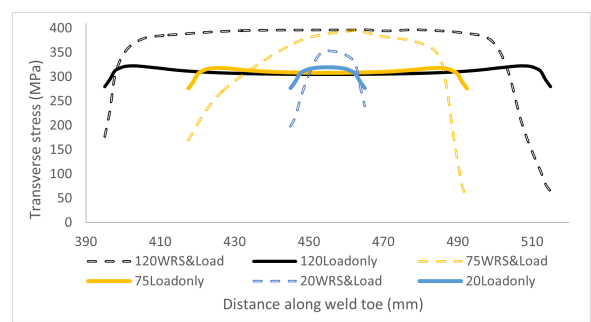


Figure 4.54: WRS & Load vs. Load only for (120, 75 and 20 mm)

Length (mm)	Max stress including TWRS (MPa)	Max stress excluding TWRS (MPa)	Difference in stress (MPa)
910	387	346	41
500	390	345	45
210	395	332	62
120	397	323	74
75	395	318	77
20	353	320	34

Table 4.9: Difference in peak stress when including and excluding TWRS in FEA

Figures 4.53 4.54 and table 4.9 shows the difference in transverse stress levels at weld toe when including and excluding welding residual stresses in numerical modelling; the stresses certainly are higher when including WRS in the specimen. However, only a max difference of 77 MPa of stress is recorded, which is a 24% max change in stress values. A minimum value in stress difference is again obtained by the 20 mm specimen, and that is due to having it almost free of WRS due to the substantial stress relief when cut from the 910 mm.

4.3.3. 2D plane stress validation

To validate the results of the transverse stress due to load only, a 2D plane stress model was performed. The results of the 2D plane stress model are compared with the stress results at the edges of the 3D model. While if a 2D plane strain model was performed, the results would be compared at the centre of the midsection of the 3D model.

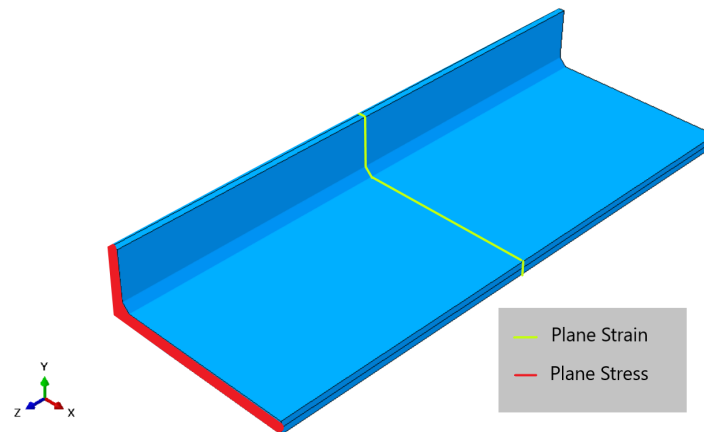


Figure 4.55: 2D plane stress & plane strain in a 3D

The transverse stress at the weld toe at the edge of $z=910$ mm for the 3D specimens are recorded and were presented in figure 4.51. These values are compared with the 2D plane stress value at the weld toe in table 4.10. The value of the 2D plane stress matches the results from the 3D model, as it gives a value of 298 MPa, which is in between the values of 500 and 210 mm specimen.

Model	Transverse stress (MPa) at $z=910$ mm
2D plane Stress	298
910	301
500	300
210	288
120	280
75	276
20	277

Table 4.10: 3D vs 2D plane stress

Figures 4.56 and 4.57 show the transverse stress S11 for the 2D and the 3D models, and show close compatibility.

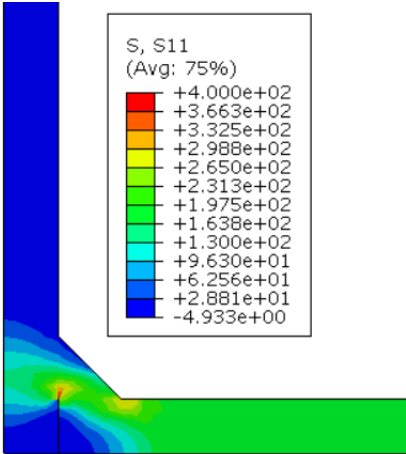


Figure 4.56: 2D Plane stress model

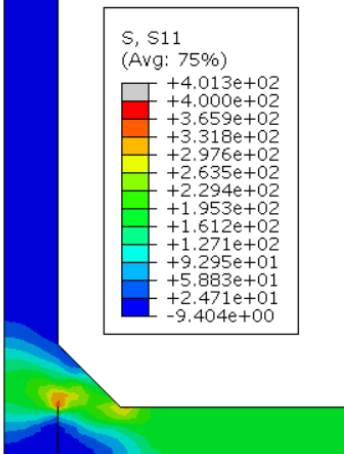


Figure 4.57: 3D model

4.3.4. Maximum Principle Stress

The results of the Max. principle stress at the weld toe due to loading + WRS and due to loading only are presented and discussed below. The stress flows for the highest tensile stresses are shown and they determine the location and direction of the crack propagation and the fatigue failure location of the specimen. The fatigue and damage can be localised, the rupture of the material can be clearly seen in a fractured specimen without the need of a microscope, as the fractured surface of a fatigue crack has a characteristic appearance.

The fractured surface for the 120 mm specimen is analysed to see the location of the constant cycles by comparing the results of the stress flow of the maximum principle stresses with the 120 mm a simple photography of the fractured specimen.

Stress due to Load and WRS

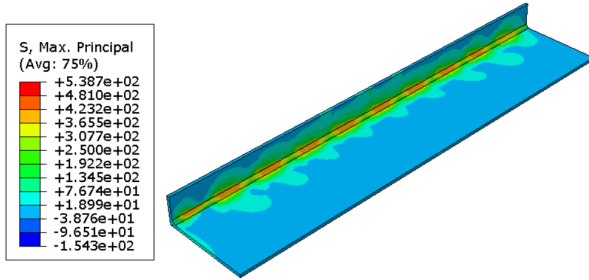


Figure 4.58: Full scale 910 mm

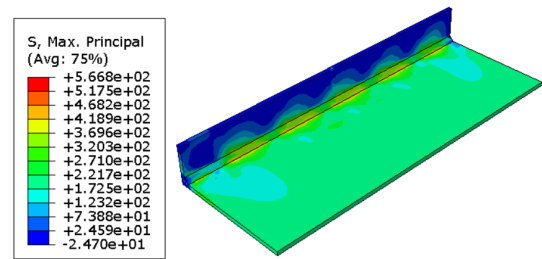


Figure 4.59: Small scale 500 mm

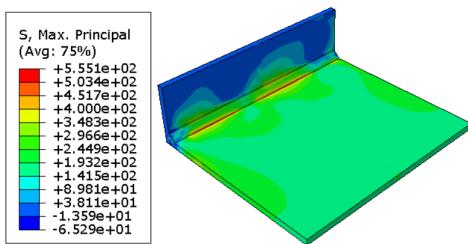


Figure 4.60: Small scale 210 mm

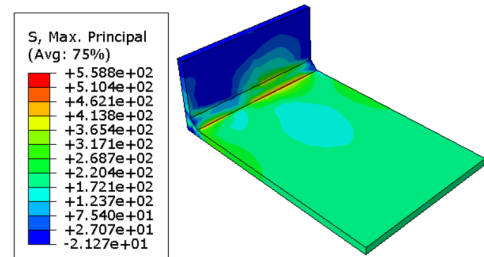


Figure 4.61: Small scale 120 mm

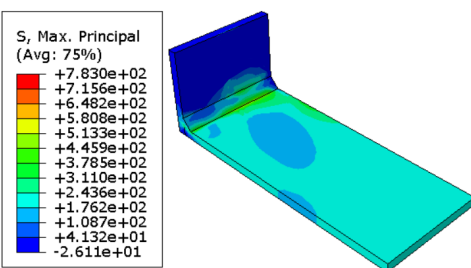


Figure 4.62: Small scale 75 mm

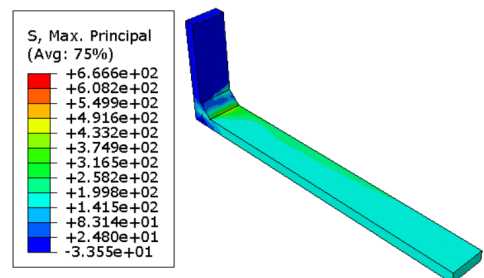


Figure 4.63: Small scale 20 mm

Max principle stress flow

It is of a great importance to analyse the maximum principle stress flows when assessing fatigue and fracture as it is a determinant for the maximum tensile stress that occur in the body. Figure 4.64 shows the direction of the max principle stress for the full scale 910 mm specimen, which in fact occurs at the weld root with an extreme tensile value of 773 MPa. This indicates that the failure of the specimen occurs at the weld root and not at the weld toe, due to the very high stresses at root location compared to the toe. However, it is important to keep in mind that this value at the weld root is a singularity that occurs due to sharp and very small size of the gap between the base and attachment plate.

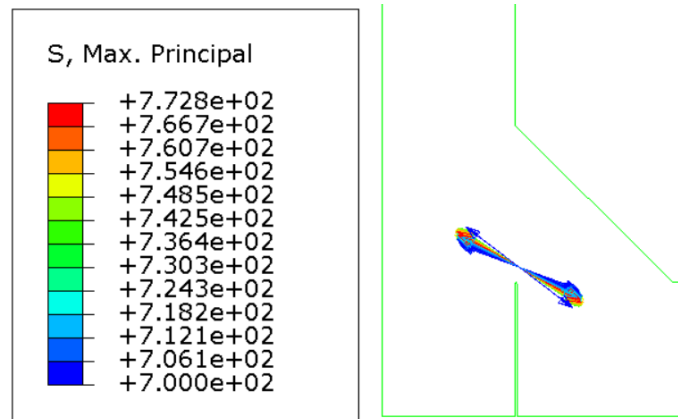


Figure 4.64: Max. Principle stress flow at the weld root

This singularity issue can be solved by creating a radius at the tip of the gap to get rid of the sharp transitions that lead to singularities, and refine the mesh in the area by having at least eight elements around the gap tip with proper element aspect ratios as shown in figure 4.65. This modification would be best applied only when having a very powerful computational capabilities, because the size of the gap between the plates is 0.05 mm, Thus many elements are needed to get the most accurate results to avoid singularities, were the total number of elements can reach up to +3 million elements causing a very large computational time for running the welding simulation that can reach up to weeks.

Another modification method that could be implemented to avoid the stress singularities is the effective notch method, which implies the creation of a circle around the weld root with a very fine mesh. The stress level at the weld root can be accurately recorded with these methods. This project inspects the stress levels at the weld toe, this modification method was avoided to save computational time and space.

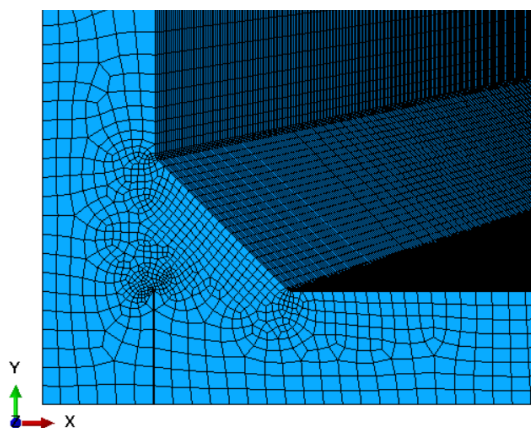


Figure 4.65: Mesh refinement

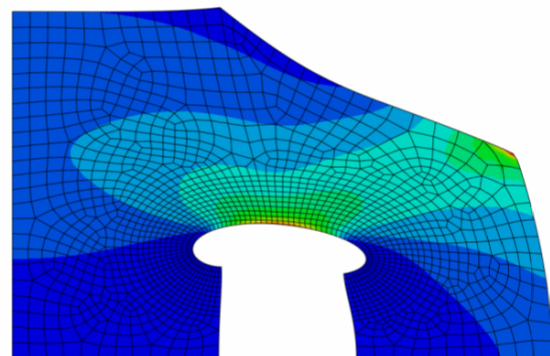


Figure 4.66: Effective notch method at root

Looking at the maximum principal stress flows for the 20 mm specimen that includes WRS and loaded under 186.2 MPa, the peak stresses occur in the midsection at the weld root and toe. extremely

high stresses occur at the weld root with values up to 666 MPa, and still very high stresses at the weld toe arise with values above the yield of 488 MPa. The final fracture however is going to occur in the weld root as the peak stresses are present there in the x-direction, which means the crack will propagate perpendicular to that. All these values are above the yield stress of 355 MPa.

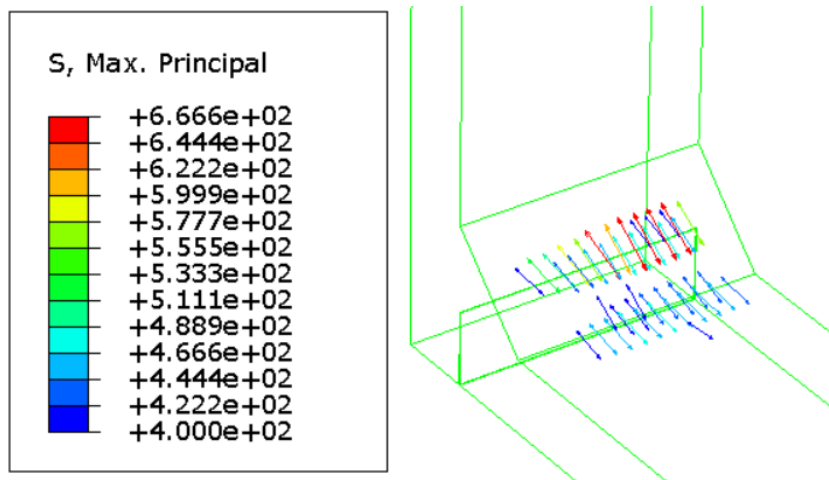


Figure 4.67: Max. Principle stress flow for the 20 mm

4.3.5. Fractured surface after fatigue testing

The 120 mm long cruciform joint specimen was studied and tested by TNO's laboratories to mainly determine the fatigue life in terms of number of cycles and investigate the phases of crack initiation and propagation and the coalescence of multiple cracks (No information regarding the welding/welding parameters were defined in the experiment). The crack initiation phase was studied by firstly evaluating a simplified fractographic using a normal camera, to then examine the fractured surface using an Electro-microscope (SEM).

In this section, the simplified image of the fatigue failure fracture will be looked at to analyse the fractured surface at the weld root, and compare it to the numerical results of the maximum principle stresses. Figure 4.68 shows the dimensions of the cruciform joint that was tested. A fatigue load with a stress range of 93.1 MPa and a stress ratio of $R=0.5$ was applied as shown in figure 4.69.

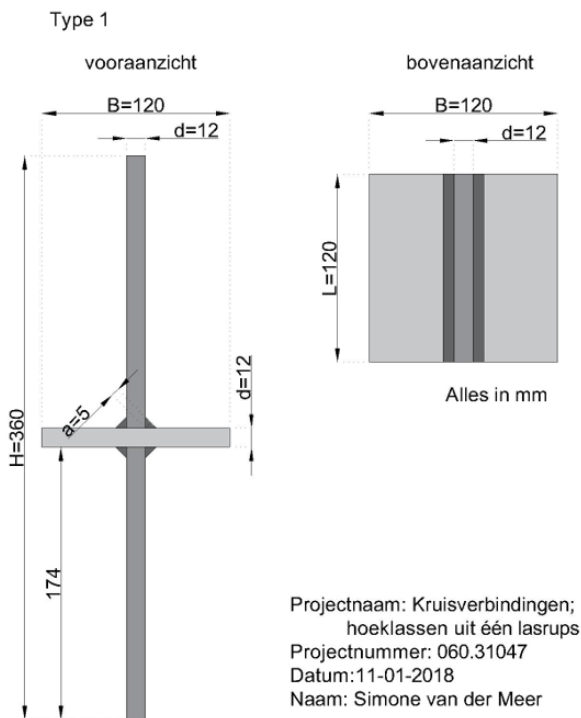


Figure 4.68: Dimensions of the 120 mm long cruciform joint specimen



Figure 4.69: Fatigue testing at TNO laboratories

After 271320 cycles a fatigue failure happened at the weld root. The fractured surface in figure 4.70 indicates that there is a smooth and brittle fractured surface. At the middle part of the specimen, it can be analysed that there is more smooth fracture due to having a constant stress range and having the applied stress taken mainly in the middle part of the specimen.

The specimen was cut down from a long welded piece to a 120 mm long specimen, so a stress relaxation happened at the edges. As mentioned, a big part of the fatigue performance is attributed to the tensile residual stress, where the peak tensile stress is located in the mid section of the specimen.



Figure 4.70: Detected crack initiation with simple photography test by TNO [12]

Figure 4.71 shows the maximum principal stress flow for the model that excludes WRS but has stresses due to load only, and figure 4.72 shows the stress flow due of the load and WRS, and both figures are for the 120 mm specimen, which is the specimen length used in experiments in the TNO laboratories. The 120 mm specimen was tested under fatigue has given to have the final fracture mainly to happen in the centre of the weld root due to the shape of the fracture and having more smooth surfaces there. Thus, figure 4.72 also predicts that the failure to occur in the central part of the specimen at the weld root. However, the comparison between figure a 4.71 and 4.72 shows the difference in location of the crack. The model that excludes WRS shows a more stress flow from the weld root that takes place from the sides of the specimen, while the the model that includes WRS, and is in fact more accurate to real welded specimens shows to have the fracture is to occur in the centre of the specimen at the weld root. This is another reason why including the effect of welding residual stresses in numerical modelling for accurate fatigue performance in vital.

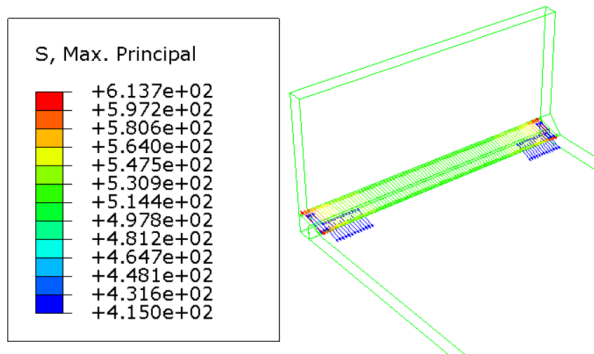


Figure 4.71: Max. Principle stress flow due to Load only for the 120 mm

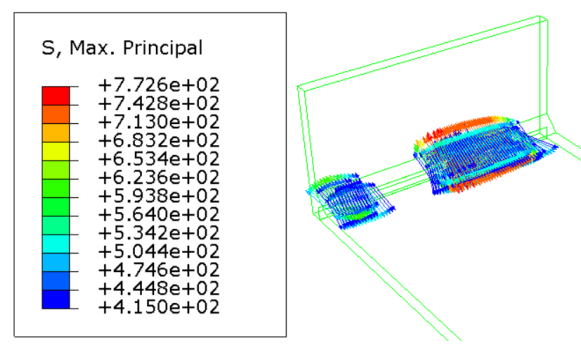


Figure 4.72: Max. Principle stress flow due to load and WRS for the 120 mm

5

Conclusions and recommendations

Before stating the main findings of this project, it is important to state the possible improvements that can make the main results more reliable.

5.1. Possible improvements

Numerous mistakes and oversimplifications happened during this study, which had an impact on the outcomes. The following adjustments could result in more accurate and realistic results:

- It is more convenient to model the full geometry of the cruciform joint when analysing the heat affected zone from the thermal model, since the thickness of the material is a major contributor of the heat affected zone. So, modelling of the full cruciform joint geometry with a fine mesh around the weld region would generate an accurate size for the heat affected zone. The thermal model did not include symmetry conditions, so the temperature field obtained is for an L-shaped specimen and not a cruciform joint.
- To predict a more accurate residual stress field, it is crucial to have sufficient mechanical boundary conditions and not over-restrain the deformation of plates due to welding. The boundary conditions can be improved by releasing restraining the z-direction from the corners of the plates only, and not along the whole edges of the plates.
- Perform a mesh sensitivity analysis to see the variation in stress around the sharp locations (the weld toe and root) to decrease the amount of discontinuities at those regions.

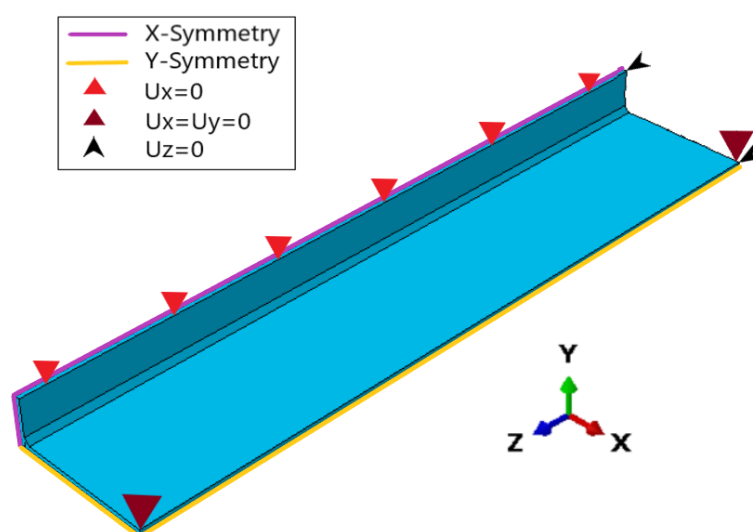


Figure 5.1: Improved mechanical boundary conditions compared to figure 3.10

5.2. Conclusions

As full scale cruciform joint specimens exhibit different characteristics than the small scale ones due to residual stress difference, the welding residual stress (WRS) distribution for the full scale 910 mm long load-carrying cruciform joint specimen that was obtained by performing a welding simulation, was investigated and examined at the weld toe after breaking it down into small-scale specimens that were analysed with and without a 186.2 MPa load. The main findings of this thesis are as follows:

- Performing a welding simulation with a one fully clamped edge and another with a free edge in the z-direction will generate up to 47% higher residual compressive stresses at the fully clamped edge.
- The removal of the mechanical boundary conditions in the mechanical model after the cooling of the weld material causes a stress relaxation of 7% in the longitudinal tensile residual stress and an increase in longitudinal compressive stress of 127 MPa and 64 MPa for the fully clamped and the free edge respectively.
- A small difference of 5% in longitudinal tensile residual stresses (LWRS) when cutting down the full scale 910 mm to 500 mm; meaning that the 500 mm exhibits the same characteristics of a full scale specimen in the longitudinal direction. A 16% and a 5% change in tensile stresses for the transverse and maximum principle stresses respectively when going cutting to 500 mm specimen. When assuming that no defects or other imperfections occur, then the behaviour of the 910 mm and 500 mm is similar and would give a similar fatigue performance. It is sufficient to conclude that a 500 mm long cruciform joint can be considered as a full scale specimen to be tested under fatigue to have reliable fatigue life assessment.
- A stress loss of 97% of welding residual stresses when the full scale 910 mm long specimen is cut to a 20 mm long specimen making it free of residual stresses. 406 MPa tensile stress loss and 190 MPa compressive stress loss at the edges reaching a plane stress condition by having a -3 MPa stress at the edges. However, 81% tensile transverse and a 77% tensile maximum principle stress loss occurred. A 20 mm specimen would give very different fatigue performance and give non conservative fatigue assessment.
- Applying a max tension stress of 186.2 MPa increases the stress at the weld toe up to 82% in the transverse direction, which is also the direction of the applied load. The increase of stress at the weld toe is more effective for the smaller specimens as the load gets more concentrated due to having less area. Nevertheless, a slight decrease of 25 MPa and 100 MPa in tensile and compressive longitudinal stress, respectively, for the 910 and 500 mm specimens due to having higher deformation in the z-direction at the edges when the load is applied in the x-direction due to the effective Poisson's effect when having larger length with a small thickness (plate-like behaviour), which introduces small compressive in the z-direction that will lower the tensile stresses in the specimens.
- When analysing the stress due to load only (excluding WRS), the longitudinal stresses shows peaks at the edges for the 910, 500, and 210 mm long specimens due to having a high L/t ratio which gives higher deformations in the z-direction when loaded in x-direction due to Poisson's; the longitudinal deformation U_z for the longest specimen is $U_z = 0.108$ mm, and a deformation of $U_z = 0.0044$ mm for the 20mm specimen causing a smaller longitudinal stress. The transverse stresses show the peak stresses at the edges for all specimens due to having a high stress concentration due at the tip of the gap between the base and attachment plate; the 20 mm specimen has the peak transverse stress in the centre due to having a small area which causes a uniform deformation as the load gets more concentrated. A 2D plane stress model was made to validate the stress level at the edge of the 3D model and showed compatible results.
- Comparing the stress levels at the weld toe between the FE models that included and excluded WRS showed large differences in longitudinal direction when loaded under 186.2 MPa. A difference of 282 MPa longitudinal stress difference for the 910 mm specimen, which means a completely different behaviour and non-conservative fatigue assessment in this direction. The longer the specimen, the larger the difference between the FE models that include and exclude WRS because the smaller specimens relax more in WRS when are cut down. The 20 mm specimen gives almost a similar longitudinal stress difference since it's almost free of WRS. The transverse and maximum

principle stress differences are not as large as the longitudinal, as they represent the stress level in the direction of the applied load.

- The maximum principle stress flow for all models occurred at the weld root and not the weld toe due to the singularity that appears from the small sharp gap between the base and attachment plate that gave very high stress values. The models that excluded WRS had the maximum principle stress flow at the edges of the weld root, but including WRS in the FE models shows to have the maximum stress flow at the middle part at the weld root, which is similar to the location of the fractured cruciform joint that was tested in the laboratories.

5.3. Recommendations

The following recommendations are stated to continue and improve on this research:

- This project lacked major validation of results which makes them unreliable. It is recommended to validate the results of the welding simulation by either performing welding experiments to measure the residual stresses or by performing a welding simulation to a specimen with welding data from literature to have a platform of comparison to be able to validate the results. When validating with welding experiments, the same boundary conditions, material properties, welding method, weld order and many other factors must be used. The thermal model in the welding simulation can be validated by comparing the size of the heat affected zone with an etched surface of real welded fillet weld specimen, while the residual stress from the mechanical model can be compared to the stresses generated from the strain gauges at the surface near the weld toe, which measure the strains when the material is expanding and contracting.
- A full cruciform joint includes four welds, however this research was done by performing a welding simulation for one weld seam only. The effects and distortions that occur for this weld are perfectly mirrored to the other welds causing a perfect symmetry, and causing the welding process to start at the same exact time for each of the four welds without considering a welding order; this has an effect on the distortion of the specimen.
- This research did not consider the cutting induced residual stresses which can have a big effect on the residual stress field, and since there are different machining methods such as milling, laser cutting etc., it is recommended to include such processes to give a higher accuracy of the stress fields induced by them. This could predict a more accurate residual stress distribution in real components.
- Include manufacturing imperfections such as modelling defects and pores along the weld seam using a random distribution tool and sizer to give a more realistic weld situation as to reality.
- Perform a parametric study on the effect of the mechanical boundary conditions in the z-direction to be able to assess the full effect of the over-restriction. and a parametric study to compare the behaviour of a full and a quarter cruciform joint.
- Include fatigue assessment by calculating the fatigue life using the effective notch method or linear elastic fracture mechanics. This will show the fatigue life in terms of number of cycles per specimen length. It is recommended to use linear elastic fracture mechanics by modelling a crack initiation and propagation life in the weld region. The number of cycles can then be calculated by measuring the stress intensity factor at the tip of the crack and including the residual stresses around it. The number of cycles can be measured for every specimen length to see how the fatigue assessment changes when each specimen is cut down.

References

- [1] Arvid Maarleveld. *Welding induced residual stresses in a segment of an orthotropic steel deck*. Tech. rep. Delft, NL.: Delft University of Technology, May 2022.
- [2] S J Maddox. *Fatigue strength of welded structures*. Cambridge, England: woodhead, 1991.
- [3] A.N.Ezeilob G.A. Webstera. "Residual stress distributions and their influence on fatigue lifetimes". In: *International Journal of Fatigue* 23 (September 2001).
- [4] Reza Haghani, Mohammad Al-Emrani, and Mohsen Heshmati. *Fatigue-Prone Details in Steel Bridges*. Tech. rep. Sven Hultins Gata 8, 41296 Gothenburg, Sweden: Chalmers University of Technology, Nov. 2012.
- [5] Marije Deul, Paula van Lieshout, and Noud Werter. *On the validity of using small-scale fatigue data to design full-scale steel welded structures: testing assumptions on residual stress relief*. Tech. rep. Delft, NL: TNO, 2022.
- [6] DNV-GL. *Fatigue assessment of ship structures*. Tech. rep. Class Guideline DNVGL-CG-0129, DNVGL, 2014.
- [7] DNV-GL. *Fatigue design of offshore steel structures*. Tech. rep. recommended Practice DNVGLRP-C203, DNV-GL, 2016.
- [8] A. F. Hobbacher. *Recommendations for Fatigue Design of Welded Joints and Components*. Tech. rep. IIW Collection. Springer International Publishing, 2016.
- [9] BSI. *Guide to fatigue design and assessment of steel products*. Tech. rep. OCLC: 879854706. London: BS 7608:2014. BSI : BSI Standards Limited, 2014.
- [10] NEN. *Eurocode 3: Design of steel structures - Part 1 - 9: Fatigue*. Tech. rep. Delft, The Netherlands, Dutch standard NEN-EN 1993-1-9, NEN, 2006.
- [11] Dongpo Wang Rui Zhan. *Evolution of welding residual stresses involving the cutting process and its effect on fatigue performance*. Tech. rep. China: School of Materials Science and Engineering, Tianjin University, 2022.
- [12] Dr. A. Manai PhD. *Statistical analysis of fatigue crack coalescence*. Tech. rep. Delft: TNO, Jan. 2021.
- [13] Laura Āboltiņa. *Modelling fatigue crack propagation in coped beams using XFEM*. Tech. rep. Delft, Netherlands: Delft University of Technology, 2022.
- [14] Inge Lotsberg. *ASSESSMENT OF THE SIZE EFFECT IN FATIGUE ANALYSIS OF BUTT WELDS AND CRUCIFORM JOINTS*. Tech. rep. Oslo, Norway, 2014.
- [15] N. Suzuki A. Ohta Y. Maeda. "RESIDUAL STRESS EFFECT ON FATIGUE STRENGTH OF NON-LOAD-CARRYING CRUCIFORM WELDED JOINTS OF SM570Q STEEL FOR WELDED STRUCTURES". In: *National Institute for Materials Science* 46 (November 2002).
- [16] Tony Abbey. *Simplifying FEA Models: Plane Stress and Plane Strain*. 2022. URL: <https://www.twi-global.com/technical-knowledge/faqs/residual-stress#WhatCausesResidualStress> (visited on 2022).
- [17] P J Withers. "Residual stress and its role in failure". In: *IOP Science* 1 (2009), pp. 2227–2231.
- [18] Jaap Schijve. *Fatigue of Structures and Materials*. 2nd ed. ISBN: 9781402068072. DOI: 10.1007/978-1-4020-6808-9, 2008.
- [19] R. Nobile V. Dattoma M. De Giorgi *. *On the evolution of welding residual stress after milling and cutting machining*. Tech. rep. Italy: Universita' di Lecce, 2006.
- [20] Henry J.Prask Thomas Gnäupel-Herold Ben T.Yen Sougata Roy Xiaohua Chenga John W.Fisher. "Residual stress modification by post-weld treatment and its beneficial effect on fatigue strength of welded structures". In: *International Journal of Fatigue* 25 (2003).

- [21] Philipp Rettenmeier, Eberhard Roos, Stefan Weihe. "Fatigue analysis of multiaxially loaded crane runway structures including welding residual stress effects". In: *International Journal of Fatigue* 82 (2016).
- [22] Yun Luo, Shugen Xu, Jian-Ming Gong, Shan-Tung Tu, Xue-fang Xie, Wenchun Jiang. "A model to predict the relaxation of weld residual stress by cyclic load: Experimental and finite element modeling". In: 95 (2017).
- [23] Donald Knuth. *SIMULEON 2022 - ABAQUS CAE*. URL: <https://www.simuleon.com/simulia-abaqus/>. (Version: ABAQUS 2021).
- [24] N.J.H. van den Berg. *Effects of residual stresses on the fatigue crack propagation of an orthotropic steel bridge deck*. Tech. rep. Delft, NL: Delft University of Technology, May 2020.
- [25] Ethan Bale. *Multipass Welding: All You Need To Know*. 2022. URL: <https://mewelding.com/multi-pass-welds/#:~:text=As%20the%20name%20suggests%2C%20multipass,to%20a%20single%20pass%20weld>. (visited on 06/12/2022).
- [26] Mehdi Akhlaghi, John A. Goldak. *Computational Welding Mechanics*. Ottawa, Canada: Springer, 2005.
- [27] TWI Ltd. *WHAT IS THE HEAT AFFECTED ZONE (HAZ)?* 2022. URL: <https://www.twi-global.com> (visited on 2022).
- [28] P. Chevriera, A. Tidub, B. Bolleb, P. Cezarda, J.P. Tinnesa. "Investigation of surface integrity in high speed end milling of a low alloyed steel". In: *Journal of machine tools and manufacture* 43 (2003).
- [29] M. HEI-Axir, M.M. El-Khabeery. "Experimental techniques for studying the effects of milling roller-burnishing parameters on surface integrity". In: *Journal of machine tools and manufacture* 41 (September 2001).
- [30] Fitzpatrick M.E.c; Sidhom H.a, Ghanem F, Braham C. "Effect of near-surface residual stress and microstructure modification from machining on the fatigue endurance of a tool steel". In: *Journal of materials engineering and performance* 11 (December 2002).
- [31] Kurt; DeVor R.E.; Kapoor S.G. Jacobus. "Machining-induced residual stress: Experimentation and modeling". In: *Journal of manufacturing science and engineering* 122 (February 2000).
- [32] D.K. Aspinwall, A.L. Mantle. "Surface integrity of a high speed milled gamma titanium aluminide". In: *Journal of materials processing technology* 118 (December 2001).

A

Appendix A: DFLUX code

The Dflux subroutine code is written using FORTRAN to define the moving the Goldak double ellipsoid heat source for a 1 pass welding process. The coordinates were defined to allow a movement in the z-direction with a rotation of 45 degrees.

```
SUBROUTINE DFLUX(FLUX,SOL,KSTEP,KINC,TIME,NOEL,NPT,COORDS, 1 JLTYP,TEMP,PRESS,SNAME)
INCLUDE 'ABA-PARAM.INC'
DIMENSION FLUX(2), TIME(2), COORDS(3)
CHARACTER*80 SNAME
!Coordinates
X=COORDS(1)
Y=COORDS(2)
T=TIME(2)                                !Total time
!initial starting point x0,y0,x0 - this depends on where your coordinate system is
X0=0.0
Y0=0.0
Z0=0.0
Current=26
Voltage=600
q1=Current*Voltage*1000                    !power
PI=3.141593
V=10.0000                                  !Speed
WeldLength=910.00
!CoolingTime=500
!coefficients from welding process equations (GOLDAK HEAT SOURCE)
a=5.0                                       !Weld dimension mm
b=5.0                                       !weld throat (mm)
cr=11.6                                    !Rear part of ellipsoid
cf=5.0                                     !Front Part of ellipsoid
ff=0.7                                     !heat input fraction front
fr=1.3                                     !heat input fraction rear
ETTA=0.95                                  !efficiency factor
Q=((ETTA*q1*6*(3**0.5))/((a*b)*(PI**1.5))) !Gaussuan heat distribution
!equation of the Arc movement (the welding is going along z direction in this case)
XC=X0
YC=Y0
ZC=Z0+V*T                                  !length= V*T
```

```

!Axis Rotation
WeldingAngle = 45.000
theta = WeldingAngle*PI/180.00
ZL = ZC
XL = XC*cos(theta) + YC*sin(theta)
YL = -1.0*XC*sin(theta) + YC*cos(theta)

IF (T<=WeldLength/V) THEN IF (Z<=ZL) THEN IF((((Z-ZL)**2)/(cr**2)+((X-XL)**2)/(a**2)+((Y-YL)**2)/(b**2))<1))
THEN FLUX(1)=Q*(fr/cr)*EXP(-3*(((Z-ZL)**2)/(cr**2)+((X-XL)**2)/(a**2)+((Y-YL)**2)/(b**2))) END IF C
Front ELSEIF (Z>ZL) THEN
  IF((((Z-ZL)**2)/(cr**2)+((X-XL)**2)/(a**2)+((Y-YL)**2)/(b**2))<1)) THEN FLUX(1)=Q*(fr/cr)*EXP(-
3*(((Z-ZL)**2)/(cr**2)+((X-XL)**2)/(a**2)+((Y-YL)**2)/(b**2)))
  END IF
  END IF
  END IF
  FLUX(2)=0.0
  RETURN
  END

```


B

Appendix B: Python Code for Element Sets

The python codes for the thermal and mechanical models that were discussed in chapter 3 were written to automatically divide the 10 weld increments into 10 element sets to be activated in the welding simulation process to ease the process of selecting the elements along the weld seam when having large number of elements.

B.1. Thermal Model

```
# -*- coding: mbc -*-
from part import *
from material import *
from section import *
from assembly import *
from step import *
from interaction import *
from load import *
from mesh import *
from optimization import *
from job import *
from sketch import *
from visualization import *
from connectorBehavior import *

Tol= 0.00001
Speed=10.0000
Nsteps =10
Weld-length =910.0
Step-time = Weld-length/Speed/Nsteps
WeldIncrement = Weld-length/Nsteps
Model-name = '1-Thermal'
a = mdb.models[Model-name].rootAssembly

                                tolerance
                                welding speed for automatic welding
                                Number of steps

Creating steps Pass 1
mdb.models[Model-name].HeatTransferStep(deltmx=500, initialInc=0.5,maxInc=0.5 , maxNumInc=1000000,
minInc=1e-11, timePeriod=Step-time, name='Welding-1', previous='Pre-step')
for i in range (2,Nsteps+1):
    mdb.models[Model-name].HeatTransferStep(deltmx=500, initialInc=0.5,maxInc=0.5 , maxNumInc=1000000,
minInc=1e-11, timePeriod=Step-time, name='Welding-'+str(i), previous='Welding-'+str(i-1))
```

```

for ii in range(1,Nsteps+1):
    e1 = a.sets['FullWeld'].elements
    elements1 = e1.getByBoundingBox(-4, -4, (ii-1.013)*WeldIncrement,
4, 4, Tol+ii*WeldIncrement)
    a.Set(elements=elements1, name='Weld-incr_'+str(ii))

```

Activation of elements in weld pass 1

```

for e in range(1,Nsteps+1):
    region = a.sets['Weld-incr'+str(e)]
    mdb.models[Model-name].ModelChange(name='Weld-incr'+str(e),
createStepName='Welding'+str(e), region=region, activeInStep=True,
includeStrain=False)

```

B.2. Mechanical model

-*- coding: mbc -*-

```

from part import *
from material import *
from section import *
from assembly import *
from step import *
from interaction import *
from load import *
from mesh import *
from optimization import *
from job import *
from sketch import *
from visualization import *
from connectorBehavior import *

```

Tol= 0.00001

Speed=10.0000

Nsteps =10

Weld-length =910.000

Step-time = Weld-length/Speed/Nsteps

WeldIncrement = Weld-length/Nsteps

Model-name = '2-Mechanical2'

a = mdb.models[Model-name].rootAssembly

*tolerance
welding speed for automatic welding
Number of steps*

Creating steps Pass 1

```

mdb.models[Model-name].StaticStep(initialInc=0.1, maintainAttributes=False,
maxInc=0.2, maxNumInc=1000000, minInc=1e-11, name='Welding-1', nlgeom=ON,
previous='Pre-step', timePeriod=Step-time)

```

```

for i in range(2,Nsteps+1):

```

```

    mdb.models[Model-name].StaticStep(initialInc=0.1, maintainAttributes=False,
maxInc=0.2, maxNumInc=1000000, minInc=1e-11, name='Welding'+str(i),
nlgeom=ON, previous='Welding'+str(i-1),
timePeriod=Step-time)

```

Creating sets for weld increments pass 1

```

for ii in range(1,Nsteps+1):

```

```

    e1 = a.sets['FullWeld'].elements
    elements1 = e1.getByBoundingBox(-4, -4, (ii-1.013)*WeldIncrement-
Tol, 4, 4, Tol+ii*WeldIncrement)
    a.Set(elements=elements1, name='Weld-incr'+str(ii))

```

Activation of elements in weld pass 1

```

for e in range(1,Nsteps+1):

```

```

    region = a.sets['Weld-incr'+str(e)]
    mdb.models[Model-name].ModelChange(name='Weld-incr'+str(e),
createStepName='Welding'+str(e), region=region, activeInStep=True,
includeStrain=False)

```